POLITECNICO
MILANO 1863

SCUOLA DI INGEGNERIA INDUSTRIALE
E DELL'INFORMAZIONE

Identification of Molten Aluminium Level through Vision System in Casting Furnaces

Tesi di Laurea Magistrale in
Automation and Control Engineering - Ingegneria dell'Automazione

Emanuele Della Bosca, ID 925542

Advisor:
Prof. Marco Tarabini

Co-advisors:
Fabio Conti
Yuvan Sathya

Academic year:
2021-2022

Abstract: The accurate measurement of molten aluminium level in continuous casting processes is a major issue which affects the final product quality and process efficiency. The presented work is directed to the development of a camera vision system for the measurement of aluminium level inside a furnace. Molten aluminium surface and internal refractory walls of the furnace have different light intensity values. At the interface they form an edge which can be used to identify a line using existing machine vision techniques. An algorithm to identify the interface line and measure the melt level inside the furnace was developed. The reference system for level measurement is based on the size and relative position of known features of the furnace in the framed view of the camera. The algorithm is able to provide on-line measurement of the aluminium level for different illumination conditions inside the furnace. Field experiments showed that the method can achieve level measurements with measuring error of 6 mm at 99.7% confidence level.

Key-words: level measurement, molten aluminium level, camera system, machine vision

1. Introduction

In the continuous casting of aluminium the molten aluminium is fed from a furnace into an open mold [1, 2]. Heat is extracted from the metal which enters the cooled mold. The casting slowly exits from the open mold and is further cooled by direct application of cooling water. By means of pinch rolls the casting is slowly advanced so that a long continuous crystal can form. A schematic of the process is shown in Figure 1.

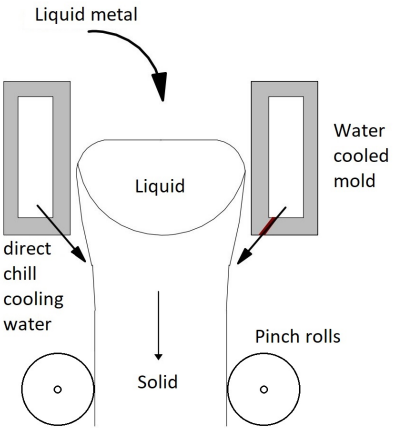

Figure 1: Schematic of the continuous casting process.

Problem statement

As stated in [1] many variables concur in the formation of the crystalline microstructure of the casting and among those temperature and flow rate play a key role. Knowing the correct level of melt in a furnace is of paramount importance to obtain the optimal liquid metal flow rate. Accurate measurement of molten aluminium level in the continuous casting processes is a major issue which affects the final product quality and process efficiency. Controlling the aluminium level is the simplest method for the improvement of the final product's mechanical properties. Moreover, a correct monitoring of the level is a desirable condition in order to avoid unscheduled stops of the plant. The stop of a casting plant translates in time consuming restart procedures and loss of profit and productivity.

Literature Search

A literature search for the existing liquid level measurement systems was performed on Scopus, Scholar and Web of Science electronic databases. Queries included keywords and Boolean logic with AND/OR operators in the form: ("liquid" OR "metal" OR "aluminium" OR "steel" OR "melt") AND "level" AND ("measurement" OR "detection" OR "control"). Particular importance was given to those articles related to casting processes. A secondary search was carried out by hand on reference lists of identified papers for additional relevant items. Primary search was conducted for publications from year 2000, limited to those articles written in English. Studies not primarily focused on liquid level measurement were excluded. Papers dealing with metal level measurement were included even if proposed methods weren't directly applied to furnaces but molds. A total of 15 articles were initially stored after primary search. Of those, 5 were discarded. One wasn't in English, two didn't provide data about accuracy and other two didn't primarily focus on liquid level measurement. After inspection of the 10 remaining articles' reference lists, 5 additional items were included. A total of 15 papers were included in the methods' review.

During the course of the research other literature searches were conducted to review techniques and methods in the field of image analysis. The focus was initially put on the state of art of line identification methods. Searches were then extended to related topics such as image processing techniques. The queries were entered in the databases in the form: ("image analysis" OR "computer vision") AND ("line" OR "edge") AND ("detection" OR "identification"). In addition the bibliographies of identified papers were hand searched. 18 articles related to the image analysis techniques used in this work were selected.

The bibliography also includes two references to papers which explain the continuous casting process, a practical manual for digital image processing and a programming functions library. A total of 37 items were included in this thesis.

Review of Existing Measurement Methods

One of the most traditional techniques to measure metal level has been the use of sounding bars [3]. In this method a metal rod made of steel is periodically immersed into the molten metal bath. Difference in colour of the rod due to heat transfer is used to determine the level. Resulting accuracy and repeatability are very

poor. This method is prone to human error and other factors such as temperature variation. The heat transfer process between molten metal and rod depends both on the temperature of the furnace and of the rod which aren't constant conditions. Moreover this method involves the presence of a human operator in hazardous conditions and measurements can't be taken frequently. Due to the high temperatures reached in the furnaces, other common contact methods for liquid level measurement [4, 5] are of difficult application. Another diffused way of estimating metal level is by weighting the solid material before it enters the furnace. This brings many sources of uncertainty. First, the refractory walls of the furnace are characterized by roughness and subject to wear. It follows that the chamber's internal volume isn't precisely measurable. Second, the metal to be melt is likely to contain other undesired materials. The level uncertainty for this method is in the order of centimeters. A similar technique using gravimetric gages cited in [6] is reported to have uncertainty up to 50 mm.

On the other hand, various non-contact measuring techniques have increasingly caught on. These techniques include γ-rays transmission [6, 7], laser triangulation [6, 8], thermal [9], Eddy current [10], induction [7], capacitance [11] and computer vision [6, 8] methods. γ-rays transmission uses a high-energy/high-penetration type of radiation which can be harmful for human body so it isn't suitable for production plants with the presence of human operators. Laser triangulation can give precise measurements but can only measure a point in the melt area, making it necessary to use an array of laser sensors to get an estimate of the level for the whole area. This can be expensive in terms of cost and system calibration effort. The use of thermocouples embedded in molds (Figure 2) is a relatively inexpensive and diffused method to measure the metal level from the temperature distribution in mold wall. In casting, the mold is the refractory structure where metal starts the solidification process. The distribution has a quite clear jump in correspondence of the melt surface. Accuracy and measuring range are, however, limited by the large gap between the thermocouples and the mold/melt interface. The proposed method in article [9] showed that with 20 mm gap, the minimum level variation that could produce a measurable 1°C temperature change was about 8 mm. Installation in the walls of a furnace is more problematic since for good sensitivity the sensors should be placed at important depths inside the refractory material, which is subject to wear. Besides, several thermocouples would be needed to get reliable measurements in the whole range where the level varies.

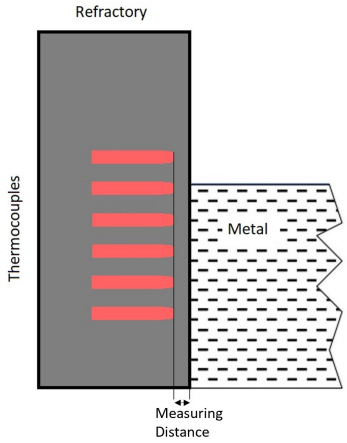

Figure 2: Thermocouples installed in mold wall.

Electromagnetic methods based on Eddy current sensors also have accuracies that highly depend on the distance of the sensor from the measured object. Due to the attenuation of electromagnetic field with distance they are effective only when the sensor is close to the object. The results reported in [10] show a RMS error of ± 11 mm at a measuring distance of 305 mm for the designed sensor in Figure 3a. Installation in furnaces walls as proposed in the paper (Figure 3b) isn't the best option since the thickness of the concrete is a constraint to the measuring distance and only a portion of the level excursion can be monitored.

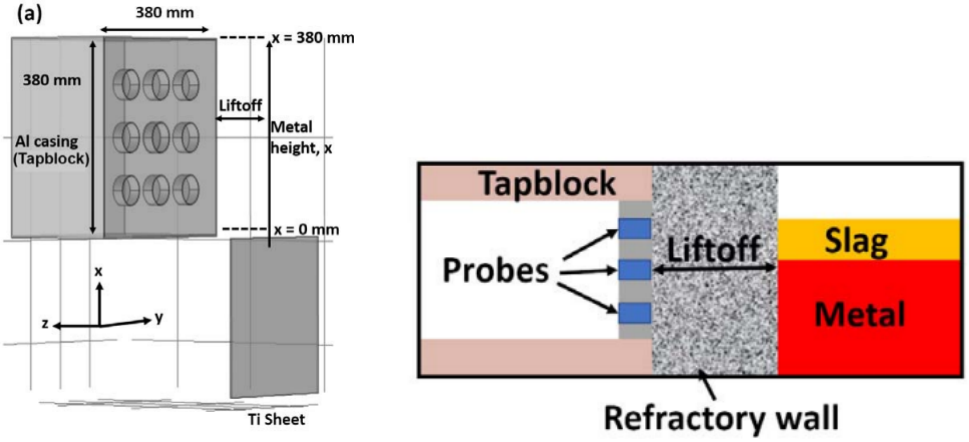

(a) The Eddy current sensor used in [10].

(b) Installation of the sensor in refractory wall.

Figure 3: The Eddy current based system in [10].

Inductance and capacitance measurement methods in [7, 11] aren't a suitable option for installation inside a furnace. To get good measurements the sensors should be placed at close distance from the melt surface as shown in Figures 4a and 4b. Application to molds of these techniques achieve very good accuracies of 1 mm for the capacitive sensor [11] and 0.2 mm for the inductive system [7]. However, eventual operation in furnaces would imply high temperatures and coming into contact with molten metal splashes. These conditions are likely to damage this kind of sensors.

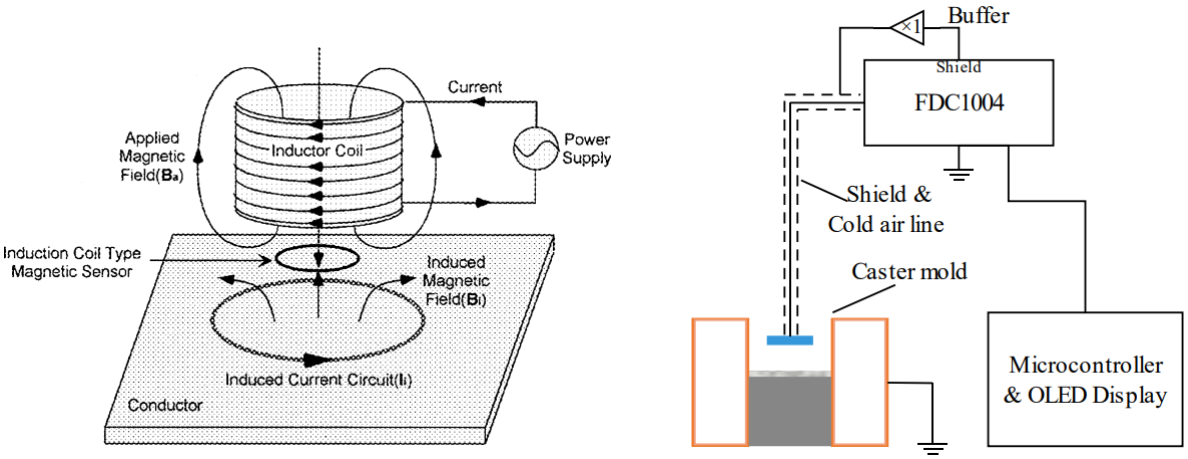

(a) The inductor coil used in [7].

(b) Configuration of the capacitive sensor in [11] .

Figure 4

A computer vision technique found in literature is used to measure steel level in tundish [6, 8]. In metal casting, a tundish is an open container of refractory material used to feed molten metal into ingot molds. The method makes use of a combination of a sounding bar, a laser for triangulation and a computer vision system. The procedure is basically an automatization of the sounding bar method. As such, it requires a mechanical system to periodically deliver the bar, which adds ulterior maintenance costs. This doesn't make it a proper non-contact method. Furthermore it still has some of the disadvantages of the traditional sounding bar method previously described [3]. The camera system is used to determine the flux/steel interface on the sounding bar through image analysis. Laser triangulation is used to estimate the thickness of the flux layer. The system is shown in Figure 5. The stated measurement accuracy is ± 7 mm at 95% confidence level.

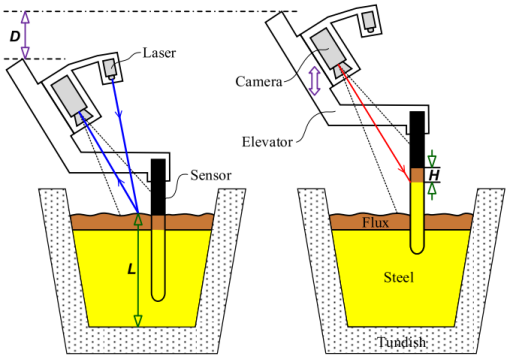

Figure 5: Measuring method based on machine vision in tundish in [6, 8]

Outside of the field of metal casting other computer vision based systems for the measurement of liquids level exist. Methods like the ones in [12–15] use a camera to measure the level of liquids against a measuring graduated scale. Another technique presented in [16] uses a circular float to measure the level inside a tank. A camera placed at the top of the tank and looking downwards captures images of the liquid surface with the float. The measured diameter in pixels of the float in the images is used to estimate the level from known relations with camera parameters. A third technique found in literature makes use of a structured illumination source with known pattern [17]. The pattern is detected with a camera system and level is computed through perspective geometry relations. The diffusion of computer vision systems for liquid level measurements makes it interesting to investigate the possibility to use such systems to measure molten aluminium level. A vision system could overcome many of the problems found in the described methods for melt level measurement. Among the advantages there would be the possibility to take measurements with good frequency and at safety distance from the melt, the no need of moving parts and the possibility to monitor extended areas.

Objectives

The work presented in this thesis is directed to the development of a camera vision system for the measurement of aluminium level inside a furnace. The camera for image collection has to be encased in the internal refractory sidewalls of the furnace, with no need of moving elements. Illumination is one of the main issues for vision systems [18, 19]. Inside a furnace many factors contribute to the chamber's light conditions. The most important are intensity of the flames from the burners, reflection of molten metal surface and temperature. If illumination isn't enough, the vision system is unlikely to be able to identify the level. In the opposite case, if illumination is excessive all intensities captured by the camera tend to be equal and the image results to be useless. As a result, the method under study is expected to perform well when the lighting conditions are met. An important step will be the pre-processing of the images [20]. The main tasks of the system to be implemented are a robust on-line level detection able to adapt to different illumination circumstances and the ability to provide a reliable measure of the molten aluminium level. The set objective for the proposed method is to achieve a measurement uncertainty in the order of ±5 mm.

The rest of the work is organized as follows. Section 2 presents the steps followed for the development of the proposed method, which include the setup of the experimental system, the system calibration, the techniques used to process the captured images and to measure the level. Section 3 presents the obtained results. In Section 4 the results and performances are discussed. Finally Section 5 summarises the main achievements of the study.

2. Proposed Method

The proposed level measurement system was designed for its operation in two different furnaces. First furnace will be addressed as "casting furnace" and is composed by a single chamber. The other furnace is composed by two chambers separated by a refractory wall. Communication between the two stages is provided by an opening at the base of the dividing wall. Raw solid aluminium scrap is loaded in the first chamber, called "cold chamber", to be melted. The opening only allows molten aluminium to flow inside the second chamber which will be addressed as "hot Chamber". The blueprints of the two furnaces are depicted in Figure 6. Illumination inside the furnaces is only provided by the flames of the burners.

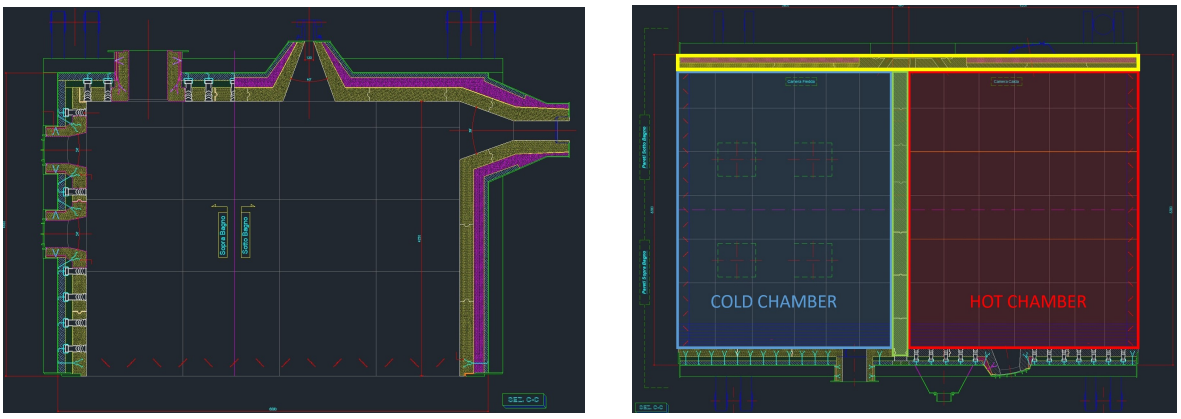

(a) The casting furnace. (b) The double chamber furnace.

Figure 6: Top view of the two furnaces.

The idea at the base of the method is that molten aluminium surface and refractory walls generally have different light intensity levels. At the interface they form a straight edge. Using existing techniques it is possible to identify lines in images [21]. Appropriate image pre-processing is required to prepare the images for level identification [20]. Through known image analysis techniques the melt surface and wall areas can be separated [18]. Level can be identified as the edge that divides the two areas. In this section the method's development steps are presented in a logical order. First, a general description of the two cameras that were used is provided in subsection 2.1. Then in subsection 2.2 a study of the cameras' positioning is conducted for the two furnaces. Subsection 2.3 describes the camera calibration procedure. Subsection 2.4 presents the pre-processing operations and the algorithm for level identification and measurement.

2.1. Hardware Setup

The hardware for image acquisition made available by the company consists of two cameras specifically designed for high temperature environments. The cameras are from the EXTREMETEMP™ furnace cameras series by manufacturer Canty (Buffalo, NY USA). This series is rated for use in applications where temperatures reach a maximum of approximately 1900°C. The cameras feature an air cooling system to keep electronics and lens protected from the harsh conditions of the furnaces. They have a cylindrical insertion length to allow the mounting inside the refractory walls of the furnaces. Accurate drawings of the EXTREMETEMP™ camera are shown in Figure 7.

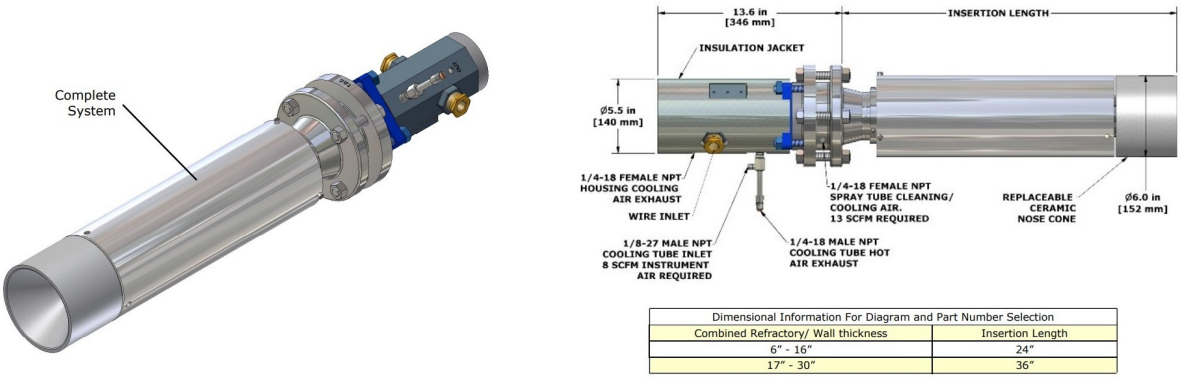

Dimensional Information For Diagram and Part Number Selection	
Combined Refractory/ Wall thickness	Insertion Length
6" - 16"	24"
17" - 30"	36"

(a) (b)

Figure 7: The Canty EXTREMETEMP™ camera

Ethernet connection provides remote access to live system images through a networked computer. The optical sensor for image acquisition is of type CCD (Charge coupled device). Various options are available for the resolution of the sensor and the lens view angle. The provided cameras are equipped with high resolution 8 MP optical sensors in the format 3840x2160 pixels. The output image is in RGB color format. Each 8 bit channel

has 256 color intensity levels. The lens has view angles of 65° and 49° in the horizontal and vertical directions respectively. The next subsection presents cameras' positioning studies.

2.2. Camera Positioning

With regards to camera positioning, two different studies had to be performed for the two furnaces. The original AutoCAD drawings of the furnaces were used in order to identify the optimal positions. A MATLAB script was created to evaluate the different possibilities. The program was built to let the user recreate a simplified 3D reconstruction of the furnace chamber. Then the camera position and orientation can be set with respect to a global system of coordinates. In addition to this, the user can choose the camera intrinsic parameters to be used by the program. The parameters include horizontal and vertical resolution of the sensor and horizontal and vertical lens view angle. Based on the classical pin-hole camera model (Figure 8) [22], the program is able to construct the 2D projection of the 3D generated points.

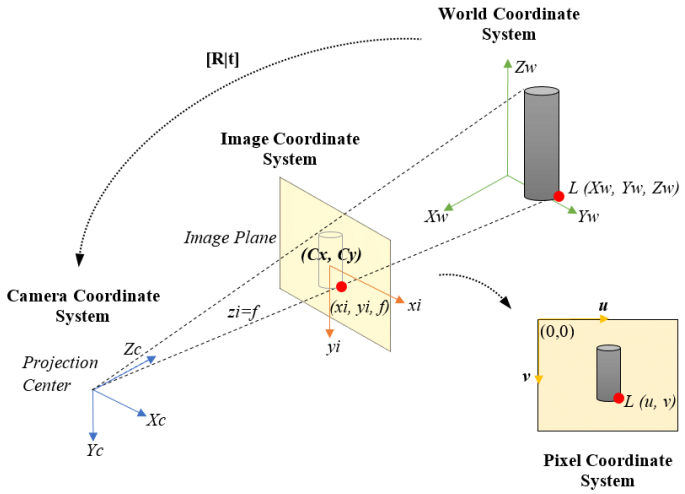

Figure 8: Simple drawing of the pin-hole camera model.

The pin-hole model equations, in homogeneous coordinates:

$$\begin{bmatrix} x_{pix} \\ y_{pix} \\ 1 \end{bmatrix} = \underbrace{\begin{bmatrix} f_x & 0 & C_x \\ 0 & f_y & C_y \\ 0 & 0 & 1 \end{bmatrix}}_{\mathrm{K}} \cdot \underbrace{\left[\begin{array}{c|c} R_w^c & t_w^c \end{array}\right]}_{T_w^c} \cdot \begin{bmatrix} X_w \\ Y_w \\ Z_w \\ 1 \end{bmatrix} \tag{1}$$

K : Matrix of camera intrinsic parameters. It defines the projection of a point in the 3D space to the 2D image plane.

T_w^c : Matrix that defines the transformation (Rotation R_w^c and translation t_w^c) from the global system of coordinates to the camera system of coordinates.

x_{pix}, y_{pix} in Equation (1) are the coordinates in pixels of the projected 3D point (X_w, Y_w, Z_w) in the image plane.

Through this transformation it is possible to have a preview of what the camera is going to frame once installed in the furnace. Some precautions were taken into account regardless the specific furnace under study. The cameras cannot be placed too close to the melt surface, otherwise molten aluminium splashes could reach the lens and damage it. In addition to this it was decided not to position them near the burners in order to keep the lenses far from the flames. The performed tests are now presented for the two distinct furnaces.

2.2.1. Casting Furnace

Figure 9 shows the top view of the casting furnace. The sides are composed by three adjacent refractory walls and a front door.

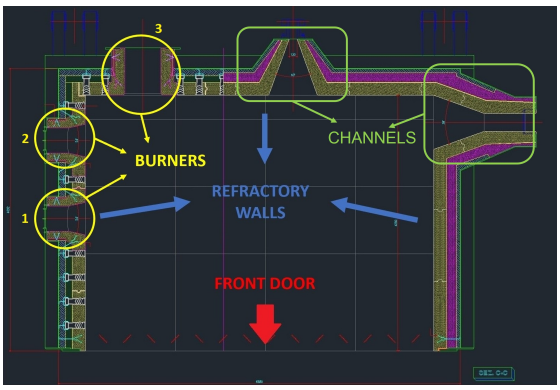

Figure 9: Blueprint top view of the casting furnace.

The camera can't be installed in the front door, which is a moving part of the furnace. Left refractory wall was also excluded because of the presence of burners 1 and 2. The burners are highlighted in yellow in Figure 9. Burner 3 operates in the leftmost part of the back wall, so also this part wasn't considered. Three positioning hypothesis were identified and compared. The maximum aluminium level reached in the chamber is about 825 mm from the refractory floor. As a safety measure an height of 1400 mm from the bottom was adopted for the three alternatives. The three positioning alternatives are presented.

Position Hypothesis 1

A first positioning hypothesis was studied with the camera in the wall to the right. Installation in the first 1200 mm from the back wall is not feasible for the presence of the entrance channel in Figure 9. Minimum allowable distance is 1300 mm. As depicted in Figure 10 the camera is rotated 30° to the right with respect to the perpendicular to the installation wall. The camera was rotated by this particular angle because the camera frame was able to capture the level of molten aluminium for the entire length of the back wall. The optical sensor is rectangular of size 3840x2160 pixel and it was rotated so that the longest side is vertical to best frame the part where level excursion occurs. Position and orientation are highlighted in Figure 10. The result from MATLAB simulation is shown in Figure 11.

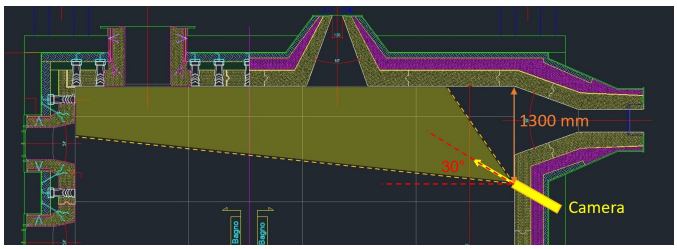

Figure 10: Positioning hypothesis 1.

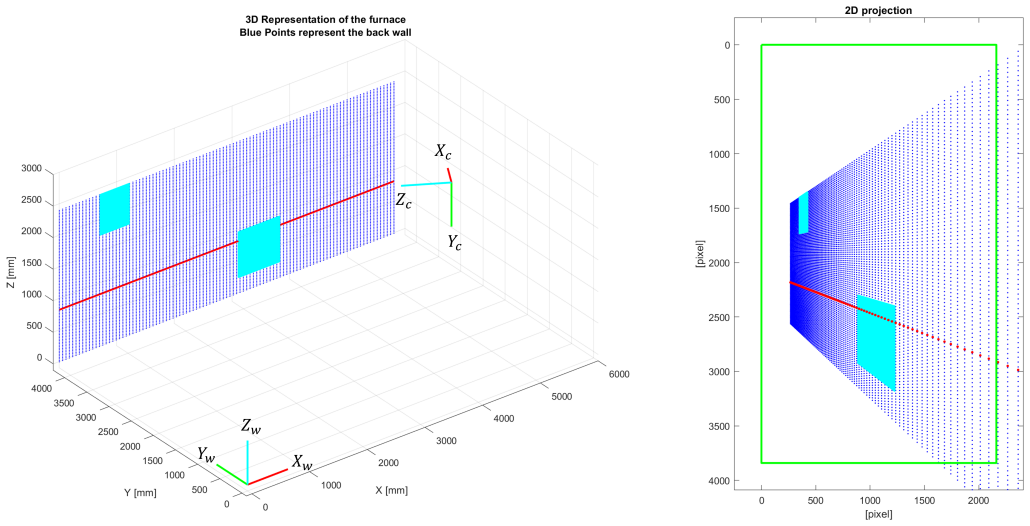

(a) 3D simulation. (b) Simulated 2D projection.

Figure 11: Simulation of position hypothesis 1 in MATLAB.

The green rectangle in Figure 11b is a visualization of the framed area of the furnace. The blue points represent the wall. The cyan rectangular features represent burner 3 and exit channel. The red line indicates the maximum level reached by the melt.

Position Hypothesis 2

Second alternative shares the same position of the first one. What changes is the rotation which is now 45° with respect to the perpendicular to the installation wall. This choice is taken to try to exclude elements of disturbance such as the burners from the resultant image. The choice for the optical sensor orientation is unvaried. Position and orientation are highlighted in Figure 12. The result from MATLAB simulation is shown in Figure 13.

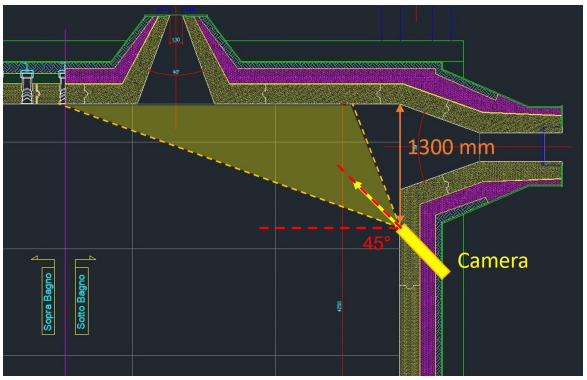

Figure 12: Positioning hypothesis 2.

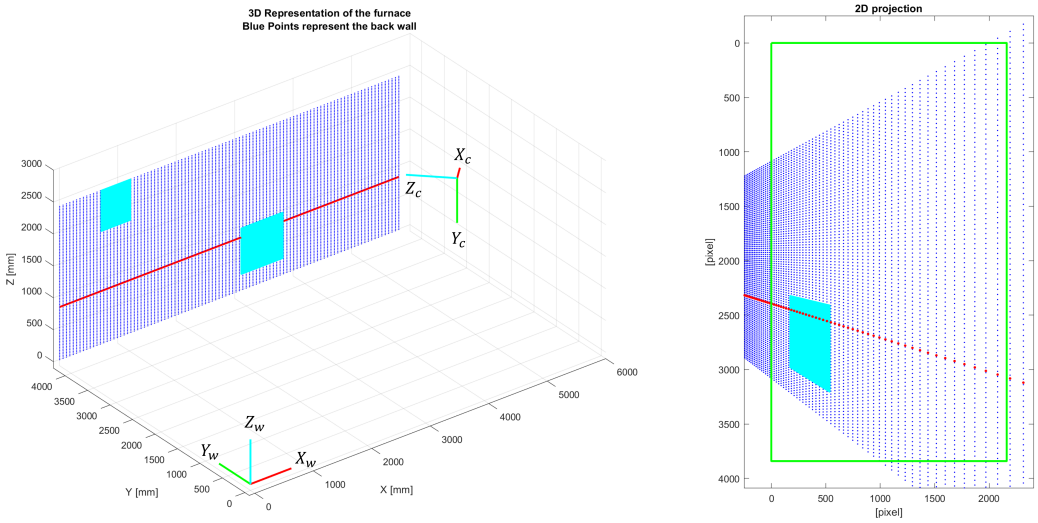

(a) 3D simulation. (b) Simulated 2D projection.

Figure 13: Simulation of position hypothesis 2 in MATLAB.

Position Hypothesis 3

A third possibility was individuated to try to completely exclude elements of disturbance. As depicted in Figure 14 the installation wall changes. The camera origin is set on the back wall at 1300 mm distance from the right wall. The rotation is 30° towards the right wall. Figure 14 shows the third configuration. The result from MATLAB simulation is shown in Figure 15.

Figure 14: Positioning hypothesis 3.

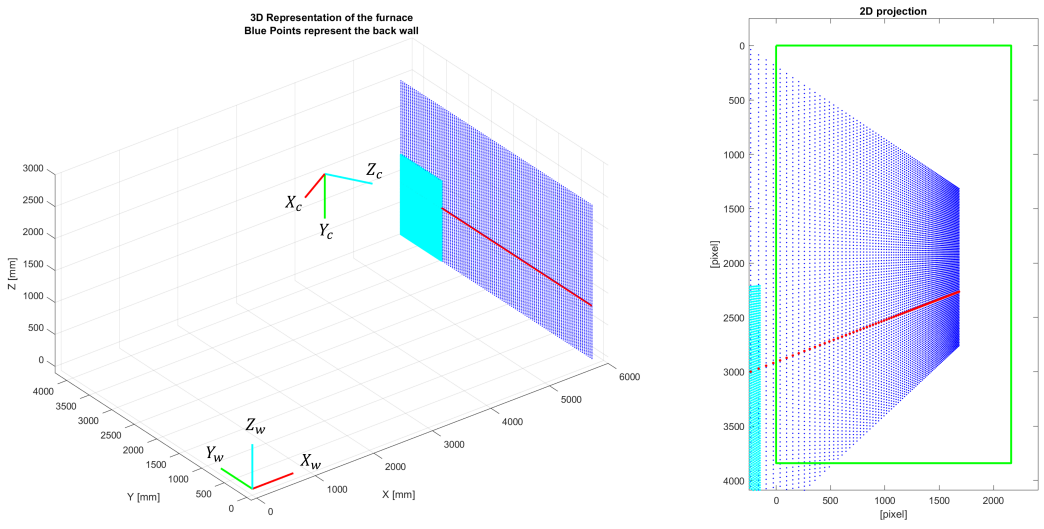

(a) 3D simulation. (b) Simulated 2D projection.

Figure 15: Simulation of position hypothesis 3 in MATLAB.

The three results were compared. Even though it was possible to see the melt level over the entire back wall length, position hypothesis 1 was discarded because of the presence of the burner in the simulated image (Figure 11b). The exit channel is an ulterior source of disturbance since it interrupts the level edge continuity. The second option resulted to be impracticable since the thickness of the furnace walls doesn't permit to install the camera with a rotation of 45°. The depth of the necessary hole to install the camera would be approximately 950 mm while the maximum insertion length of the camera is 915 mm. It was decided to proceed with third option since it didn't present the disadvantages of option 1 and 2. In the simulated view of Figure 15b it is evident that no disturbance elements are present and the level line doesn't have interruptions. The comparison between the simulation and the real image is shown in Figure 16. As can be noticed the simulated image is true to the real image.

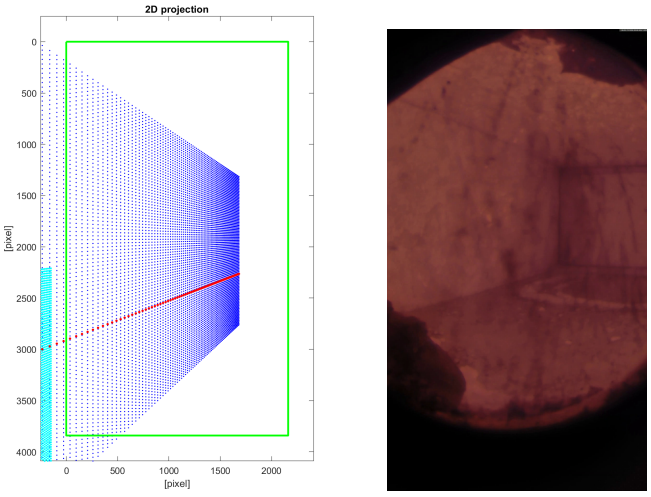

(a) Simulated view. (b) Real view.

Figure 16: Comparison between simulation and obtained image.

Remark: From now on the images from the casting furnace will be displayed mirrored with respect to the vertical axis. This is due to the camera installation procedure.

2.2.2. Hot Chamber

The second camera needs to be installed in the hot chamber. Figure 17a shows the top view of the furnace with cold (left) and hot (right) chambers. A third camera for other purposes needs to be installed in the left chamber.

To simplify the installation procedure it was decided to use one of the two perimetral walls for both cameras. The wall highlighted in yellow in Figure 17a was selected. Since positioning studies for casting furnace had been already performed, a similar configuration was adopted for the hot chamber. For the proposed positioning the camera is placed at a width of 1000 mm from the dividing wall. The melt level in the chamber reaches 700 mm. For safety the camera height is set at 1350 mm. The camera is rotated 30° with respect to the perpendicular to the installation wall towards the dividing wall. Figure 17b shows the positioning. The result from MATLAB simulation is shown in Figure 17c and 17d.

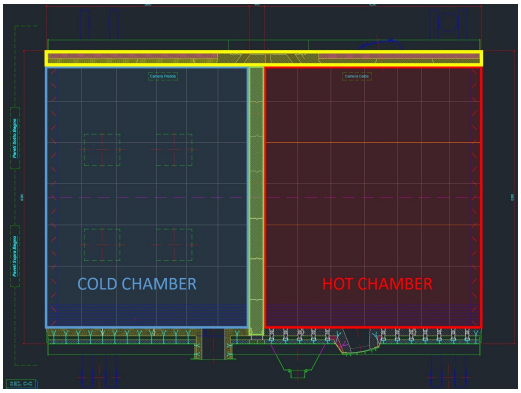

(a) Top view of the second furnace.

(b) Positioning in the hot camber.

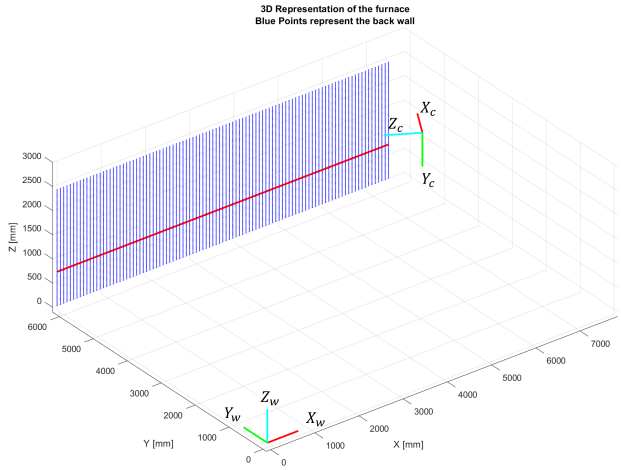

(c) 3D simulation.

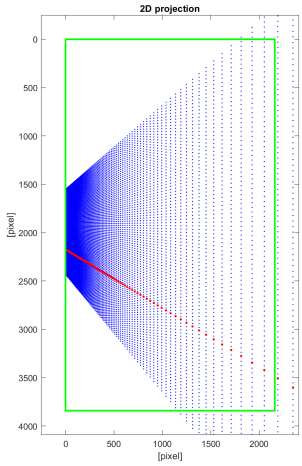

(d) Simulated 2D projection.

Figure 17: Drawings and MATLAB simulation of camera positioning for hot chamber.

Remark: At this time installation of this second camera hasn't been performed yet. For further analysis only the images from casting furnace have been used.

2.3. Camera Calibration

Before installation and operation the camera was calibrated to estimate lens distortion and intrinsic parameters. The technique presented in [23] was adopted. The equipment used for calibration includes the camera, a pc, a 5000 lumen lamp and a calibration pattern. The pattern consists of an asymmetric checkerboard of dimensions 600 mm x 840 mm. Each square has 60 mm sides. The setup for calibration requires to turn on the camera and connect it to the pc. The camera was placed on a horizontal surface. The focus distance was selected based on the positioning configuration 3 in 2.2.1 and is set to 2,6 m. It corresponds to the distance between the lens and the projection of the central point of the camera on the refractory wall as shown in Figure 18b. The checkerboard was positioned at that distance from the camera lens, well illuminated by the lamp. The setup is illustrated in Figure 18a.

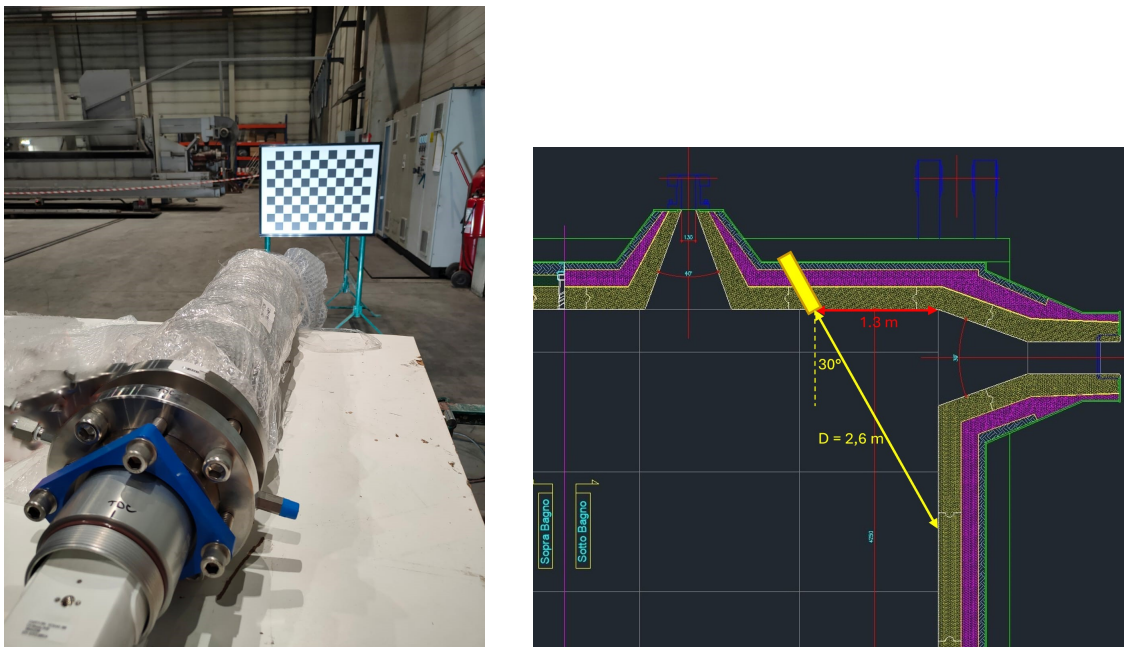

(a) The setup for calibration. (b) Calibration distance based on selected positioning.

Figure 18: The setup for calibration based on the selected positioning in the furnace.

A set of 20 images of the checkerboard at slightly different orientations and distances was taken. The set was loaded into the Camera Calibrator toolbox available in MATLAB. The application computed the camera intrinsic parameters and the coefficients for radial and tangential distortion of the lens. Figure 19 shows the checkerboard pattern before and after distortion removal. The red lines better highlight the effect of distortion removal.

(a) The distorted image. (b) The image after distortion removal.

Figure 19: Effect of distortion removal. Red lines highlight the straightening of distorted linear features

With regard to the acquisition settings, the camera captures frames at a framerate of 3 Hz with a shutter speed of 1/60 s. The decoder used is VLC.

2.4. Level Measurement Algorithm

The algorithm for level identification was developed using Python programming language. The installed Python version is the 3.7.3. The language was chosen for its versatility and open source nature. Python supports OpenCV, acronym for Open Source Computer Vision [24]. It is a library of programming functions aimed at

computer vision. It gives access to great part of the most diffused image analysis techniques. The OpenCV release is the 4.1.1. The algorithm is composed of 4 main steps: pre-processing, edge detection, line detection and level measurement. The main structure is shown in Figure 20.

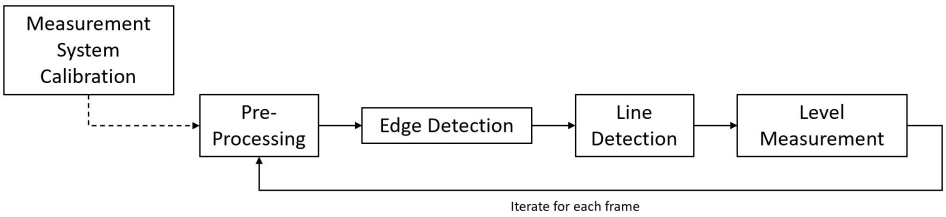

Figure 20: Structure of the algorithm.

2.4.1. Image Pre-Processing

After installation in the casting furnace it was possible to connect to the camera's live stream. Sample videos of different working conditions were collected. The untreated frames of the acquired videos were analysed under several aspects. A pre-processing strategy was developed to prepare the images for line detection. The aim of pre-processing is to improve the image data by suppressing unwanted noise and enhancing features that are considered important for further processing.

Dimensionality Reduction

In image analysis the computational effort highly depends on the dimensions of the image. Due to the construction of the optics the usable part of each frame is a circular section. The whole level excursion is visible in a reduced part of the image. Figure 21 shows two different working conditions. In Figure 21a the melt level is low while in Figure 21b it is approximately at its nominal value. The green rectangles highlight the part which is meaningful for the purpose of level identification.

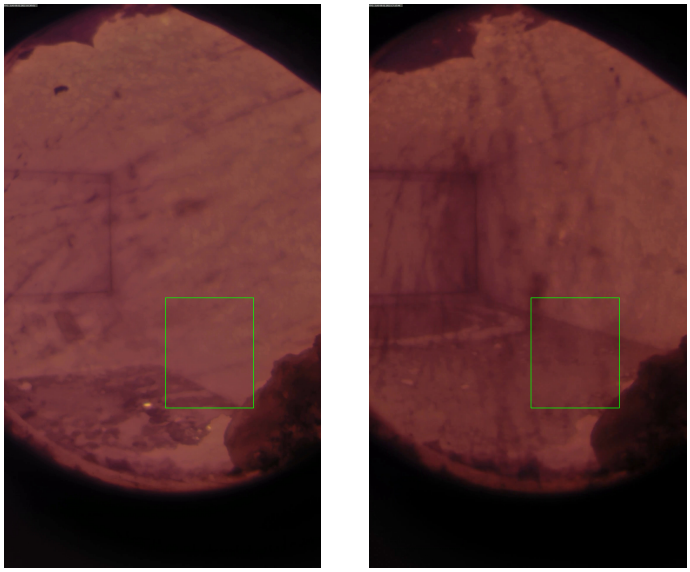

(a) Low melt level. (b) Nominal melt level.

Figure 21: Low and nominal level conditions.

It was therefore decided to perform level detection for each frame only on this cropped part. The dimensions decrease from the 2160x3840 format of the starting image to the 600x750 of the cropped image. The area is reduced by a factor of 18, cutting the processing time.

Contrast Enhancement

In order to further decrease computational effort and complexity grayscale conversion was performed for each frame [25]. The grayscale image is computed as a weighted average of the RGB values and therefore condenses

the information content of the three channels. The experimental results from grayscale conversion reported in 4.1 evidenced the need of contrast enhancement. A diffused method for contrast enhancement based on histogram modification is Equalization [26]. Equalization redistributes pixel intensities in a way that results in flattening and stretching of the original histogram. In the OpenCV library the technique is implemented by the function *equalizeHist()*.
An alternative histogram modification was developed with the aim to stretch the histogram while maintaining unaltered its shape. The idea was to apply two subsequent transformations. The sequence of modifications is shown in Figure 22.

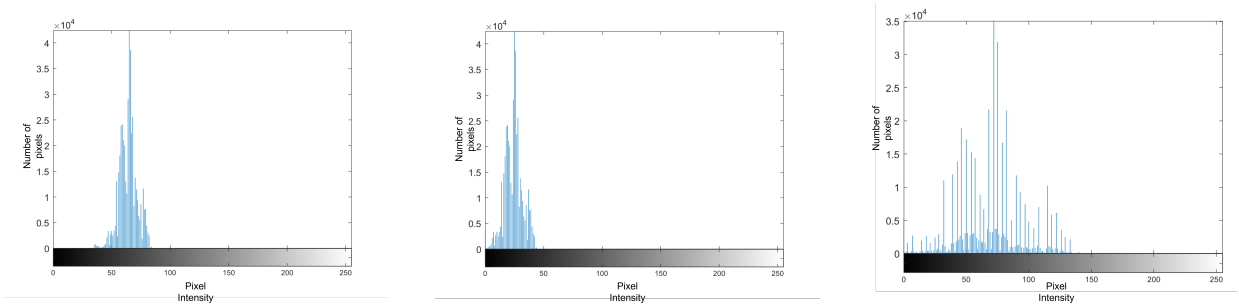

(a) Original histogram. (b) Histogram after translation. (c) Histogram after stretching.

Figure 22: Histogram modification sequence.

The first transformation is a translation of the histogram in the origin (Figure 22b). It is done by subtracting the minimum value of the range for each pixel in the starting image. The second operation consists in the multiplication of each pixel intensity for a gain in order to stretch the histogram (Figure 22c). The gain is computed starting from the difference between the maximum and minimum value in the original histogram. The rationale behind this is that the new intensity values must not exceed 255.

The formulation for transformation is:

$$o = gain \cdot (i - min) \tag{2}$$

Where o is the output pixel intensity, i the input pixel intensity and min is the minimum intensity value of the initial histogram. The $gain$ must be bounded so that o falls inside the range [0,255] as in the formula:

$$gain < 255/(max - min) \tag{3}$$

Where max is the maximum intensity value of the initial histogram.

After the testing phase, the second method was adopted over equalization. The choice is deepened in the discussion of the results in 4.1.

Noise Reduction

Edge detection techniques are easily affected by noise, so reducing the noise component in an image is fundamental [20]. Tests were carried out with different classical noise filtering techniques. They are Median blurring, Gaussian blurring [20] and Bilateral filtering [27]. The methods taken into account are based on convolution. Modification of each pixel in the starting image is done with respect to its neighbours by means of a convolution matrix, or kernel. This matrix contains weights that change depending on the specific method. Figure 23 illustrates an example of application of a 3x3 pixels convolution matrix.

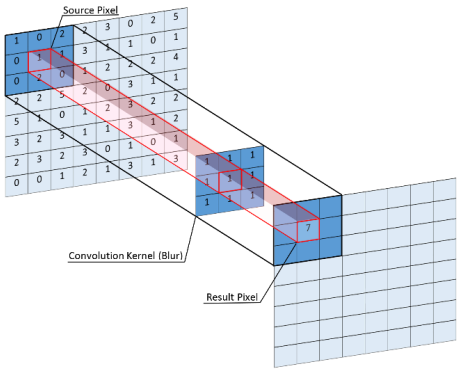

Figure 23: Example of 3x3 kernel convolution.

As a first try Median blurring was applied. The tests were performed with kernel size of 3x3. Median blurring calculates the most recurrent intensity in the neighbourhood of the pixel to modify. It then substitutes this value in the output image. Gaussian filter was tested as well. The weights of the kernel follow a 2D Gaussian distribution. More importance is given to the pixels close to the central one in the kernel neighbourhood. Kernel dimensions of 3x3 and 5x5 pixels were tested. The main drawback of the filtering techniques presented so far is that they do not depend on the specific image intensities and each pixel is processed in the same identical way. This means they blur uniform areas as well as areas that contain edges. Bilateral filter instead is a non linear, edge-preserving filter. The idea behind bilateral filtering is that two pixels can be said to be close not only in terms of spatial distance, but also if they are similar in the intensity range [28]. Two Gaussian distributions define the intensity of the filtering action. The function *bilateralFilter()* in OpenCV requires parameters *sigmaSpace* and *sigmaColor* to be tuned. The first is used to weight the spatial distance between the pixel being processed and the pixels in the neighbourhood. The second is used to weight the difference as well but in terms of pixel intensity. Bilateral filter is known to be computationally heavier with respect to the other techniques. The tests were performed using a kernel size of 5x5 pixels. It is the maximum recommended value for real-time applications in the OpenCV library.
After testing, two de-noising techniques were chosen over the others for further investigation. One is Gaussian filter 3x3 and the other is Bilateral filter. This choice is justified in 4.2.

2.4.2. Edge Detection

After the pre-processing stage the image is ready for edge detection. This step is necessary to be able to apply line recognition algorithms [21]. The classical methods used to detect borders are based on gradient computation. Those methods include Sobel, Roberts, Prewitt and Canny detectors [29]. Gradient is a measure of the difference in intensity of two pixels in a given direction. As stated in [29] Sobel, Roberts and Prewitt give comparable results so of the three only one was tested. The use of Sobel and Canny operators was evaluated. Both use convolution kernels to compute gradient in the x and y directions. The methods are included in the OpenCV library. The function *Sobel()* was applied on a set of frames to test performances. Two kernel sizes were tested, of dimension 3x3 and 5x5. On the other hand, Canny method searches for local maxima of the gradient. It uses two thresholds to detect strong and weak edges. Gradient values above *strongThreshold* are recognized as edges. Gradient values comprised between *strongThreshold* and *weakThreshold* are accepted only if they are connected to strong edges. The tests were carried out on the same set used for Sobel. The tested kernel size is 3x3. The thresholds of Canny detector are static and performances may vary from one frame to another depending on the intensity of the gradient. It was decided to investigate if an adaptive method could be used to detect borders. One of the most popular adaptive techniques for image thresholding in literature is the Otsu method [30–32]. It is based on the analysis of grayscale histogram of the image. Otsu algorithm assumes that the image histogram is composed of two principal modes, foreground and background pixels. In the images under analysis the two modes are identified with the pixels belonging to the melt area and those which belong to the refractory wall. The method uses a threshold value of intensity to divide the pixels in two classes. The threshold which minimizes the intra-class intensity variance is selected. Figure 24 shows with an example the two principal modes in a histogram.

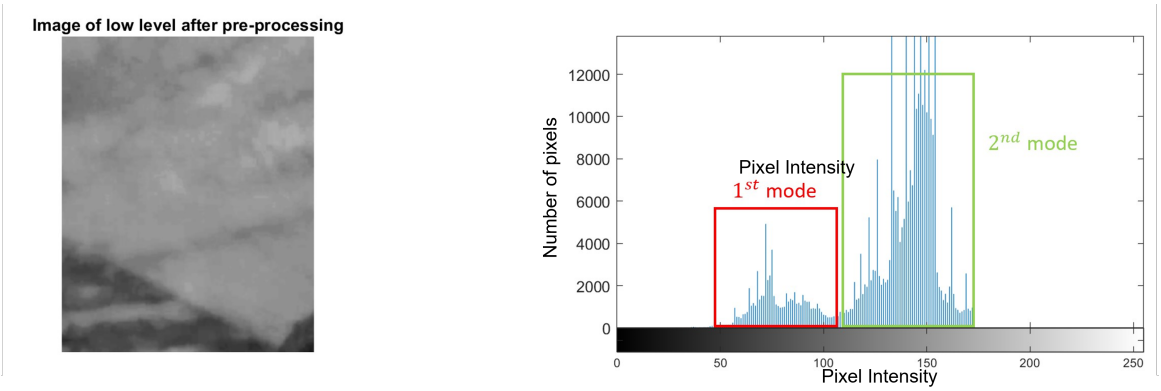

Figure 24: The two principal modes in the histogram of a pre-processed image.

The idea for the application to our case is that the level edge separates two areas in the image. The intensities of the pixels which belong to the edge are supposed to be very close to the threshold which is computed by Otsu method. Each image is binarized according to its specific Otsu threshold. All values under the threshold are set to 0 After the binarized image is obtained the edges are extracted. A schematic example of operations sequence is shown in Figure 25.

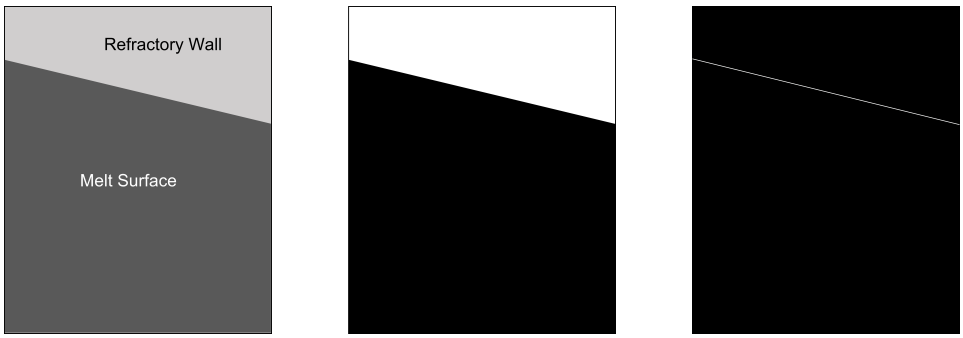

(a) Drawing of a frame after pre-processing.

(b) Binarization with Otsu threshold.

(c) Edges extracted from binary image.

Figure 25: Application example of Otsu thresholding for edge extraction.

Two different approaches were developed for edge detection. The first adopts Canny detector, the second uses Otsu method. Justification for the choice is given in subsection 4.3.

2.4.3. Line Detection

From the previous step an image containing only the edges is obtained. The next step in the proposed method is line detection. The most widely adopted technique for line detection in machine vision is the Hough Transform [21, 33–35]. This approach operates on a binary image of borders. A line in the xy plane can be described by the formula:

$$y = m \cdot x + q \tag{4}$$

However this form is difficult to manage in the case of vertical lines since $m \to \infty$. To avoid this issue Hough Transform uses a parametrization of the line known as normal form:

$$\rho = x \cdot cos(\theta) + y \cdot sin(\theta) \quad \text{-90°} \leq \theta \leq 90° \tag{5}$$

The geometrical interpretation of ρ and θ parameters is illustrated in Figure 26a. Notice in Figure 26b that a point (x_i, y_i) in the xy plane is transformed in a linear combination of two sinusoids in the so called parameter space. The example in Figures 26a and 26b shows how three aligned points are transformed in the parameter space. The point in common (ρ_0, θ_0) in the parameter space represent the common line in the xy plane. Since in reality the lines passing through a point are infinite, the computer implementation of the Hough algorithm makes use of a discretization of the parameter space [36] as shown in Figure 26c. Each cell is called accumulator

and its associated value is initially set to zero. The transformation is performed for each white pixel of the edges image. A cell value is increased each time a transformed point in the parameter plane passes through that cell. If a line is present in the image, the cell associated to the parameters of that line will have a greater count than the surrounding cells. A threshold is used to extract the cells with higher counts.

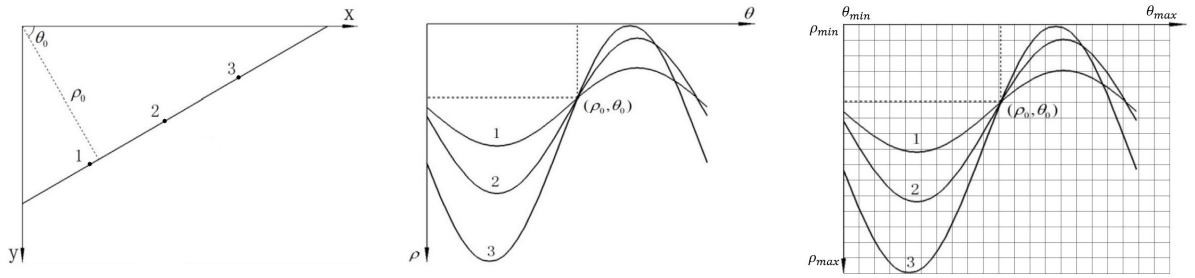

(a) Three aligned points in the *xy* plane.

(b) The parameter space. Transforms of points 1, 2, 3.

(c) Discrete parameter space.

Figure 26: The Hough Transform method.

The Hough Transform is implemented in the OpenCV library by the function *HoughLines()*. The function takes as inputs a binary image of edges, the resolutions for the accumulator cells and a threshold for the counts. It is also possible to limit the search interval for the parameter θ. As stated in [21] a fine discretization resolution results in high computation time. The resolutions were set to 1 pixel for ρ and 1° for θ. The threshold value was empirically tuned and set to 90. In order to eliminate spurious lines and reduce computation time the search is performed only over a reduced interval of θ. The tests performed showed that the interval of interest is bounded by the values [θ_{min} =100°, θ_{max} =120°]. The *HoughLines()* function returns a list of the lines that were detected. Each line is given in the form of its relative ρ and θ parameters. The list is ordered in decreasing order of the counts obtained by each line. In general Hough algorithm doesn't find a single line in correspondence of the edge but returns a few. A criterion to discard all the lines but one needs to be developed. The algorithm that was implemented to solve this problem is presented in 2.4.4.

2.4.4. Level Measurement

Up to this point of the proposed method it was possible to identify a few lines in an image in correspondence of the level edge. A calibrated reference system is needed in order to be able to provide a level measurement from a detected line. It is also necessary a procedure for the selection of a single line. First a solution for the reference system is proposed. Then the criterion for line selection is explained.

Reference System

A reference system in the image is needed to make it possible to measure the level. A paper found in literature has developed a measurement system for surfaces that uses a single camera and a square target of known size [37]. The target is used to probe the surface of the object being measured. The camera captures images of the object next to the calibrated square. Perspective projection of the square target is used to determine the 3-D coordinates of the point of contact. A re-adaptation of this method is proposed. Our camera frames the features of the furnace, whose dimensions and poses in 3D space are known. Knowledge about those features is used instead of a square target. It is pointed out that in 3D space the aluminium level lines at different heights are parallel and share the same vertical plane, identified with the refractory wall. A set of parallel lines in the 3D space is projected in a 2D image as a bundle of straight lines which converge in a single point, called vanishing point. The idea is to calibrate the system using two parallel lines and knowledge about dimensions of the furnace. The procedure is now explained. A frame where the lighting conditions are optimal is used. The line corresponding to the aluminium level is identified by a manual aided procedure. Two points are manually selected on the level edge. The two points identify a line as shown in Figure 27a. The equation of the line is computed through the two points formula:

$$\frac{y - y_1}{y_2 - y_1} = \frac{x - x_1}{x_2 - x_1} \tag{6}$$

where (x_1, y_1) and (x_2, y_2) are the pixel coordinates of the two points.

The same procedure is repeated for the edge which is formed by the refractory wall with the ceiling of the furnace as shown in Figure 27b. It is derived from the furnace measurements that this line is located at 2400 mm from the furnace floor. The two identified lines are known to be parallel in 3D space. The vanishing point can be computed as the intersection of the two lines. Notice that the vanishing point isn't necessarily inside the image area. A point is now selected on a feature located at 830 mm from the floor. It corresponds to a corner of the front door which is also co-planar with the refractory wall. The point is shown in Figure 27c. The line formed with the vanishing point is computed. This new line and the one formed with the ceiling are parallel in 3D and have a known distance of 1570 mm. The two lines can be used to derive all the other parallel lines at the desired height. The line corresponding to 0 mm was computed. The refractory wall has been mapped for the lines parallel to the level. The calibrated measurement system is shown in Figure 27d. It has been made possible to derive height measurements given the equation of a line. The proposed measurement system calibration procedure is performed offline and only once at the beginning of the algorithm. With reference to Figure 27e the formula to compute the level height of a given line is a proportion:

$$H\ [\text{mm}] = \frac{a}{a+b} \cdot 2400\ [\text{mm}] \tag{7}$$

where a and b are measured in pixel.

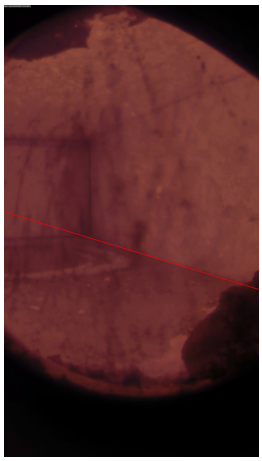

(a) The first calibration line.

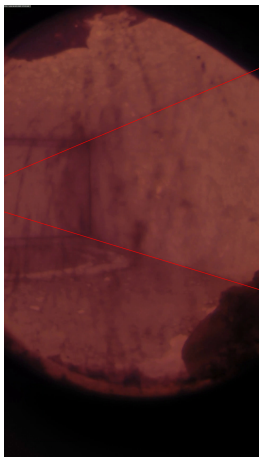

(b) First and second calibration lines.

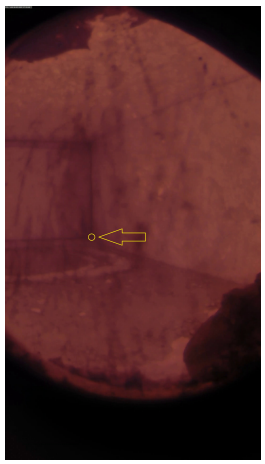

(c) The third feature used for calibration.

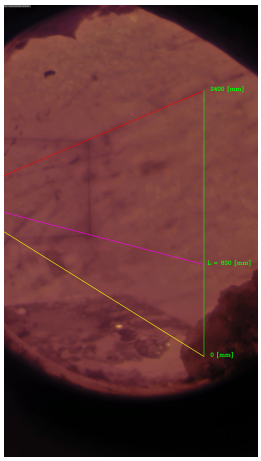

(d) The calibrated reference system.

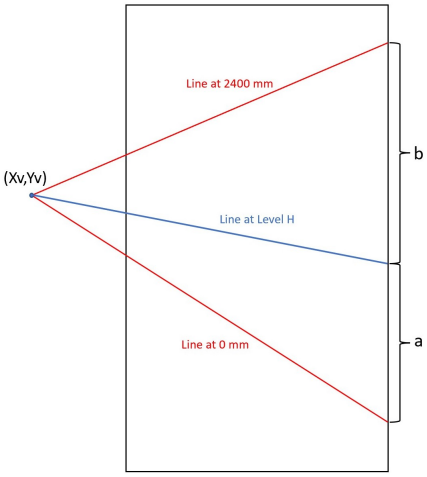

(e) Example of level measurement.

Figure 27: Calibration of the measurement system.

Line Selection Criterion

The problem of multiple lines detected by the Hough transform was solved in two steps. The first step consists in giving each line an evaluation in terms of parallelism with respect to the reference system. The area of the image where the level excursion occurs is subdivided in a set of intervals. The intervals are generated starting

from the reference system previously developed. The intervals correspond to parallel sections in 3D space. The partitioning is shown in Figure 28a. For each line detected by the Hough algorithm, if the both the extremities of the line are contained in a single interval it means the line is sufficiently parallel. It is therefore preserved. If otherwise the two extremities belong to different intervals the line is discarded. An example of the two cases is given in Figures 28b and 28c. The higher the number of intervals, the thinner they are. The number must be high enough so that only a few lines are preserved. Tuning is carried out through trial and error procedure.

(a) Intervals sketched on the cropped image.

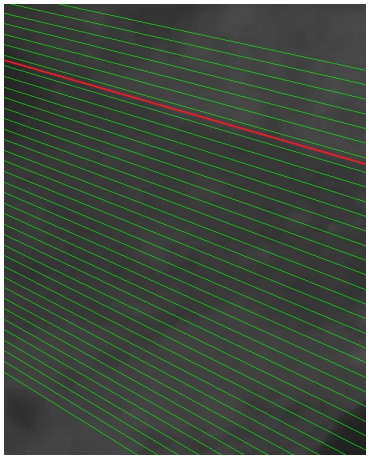

(b) Example of preserved line. The extremities of the line fall in the same interval.

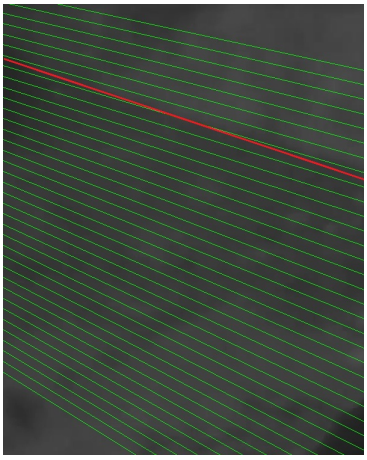

(c) Example of discarded line. The extremities of the line fall in two distinct intervals.

Figure 28: Criterion to evaluate parallelism.

Second step is based on the run-time execution of the algorithm. The melt level in the furnace is known to change with slow dynamics with respect to the acquisition rate. Therefore the level in a frame is assumed to be very close to the level in the previous frames. The information about the height of n anterior frames can be used to select a single line in the new frame. For the first n iterations of the algorithm the first line in the list of the preserved ones is selected and corresponding level height is computed. The algorithm keeps in memory the heights computed by storing them in a vector of n elements. After the first n iterations the vector is used to compute the mean value of the n previous heights. Height is computed for all the preserved lines of the current frame. The line with height closer to the mean value is selected. The vector is updated at each iteration. The oldest value in the vector is removed and the new height is added at the end. The selected line at each iteration is sketched in the output image together with the measured height value in [mm] for visual monitoring as shown in Figure 29.

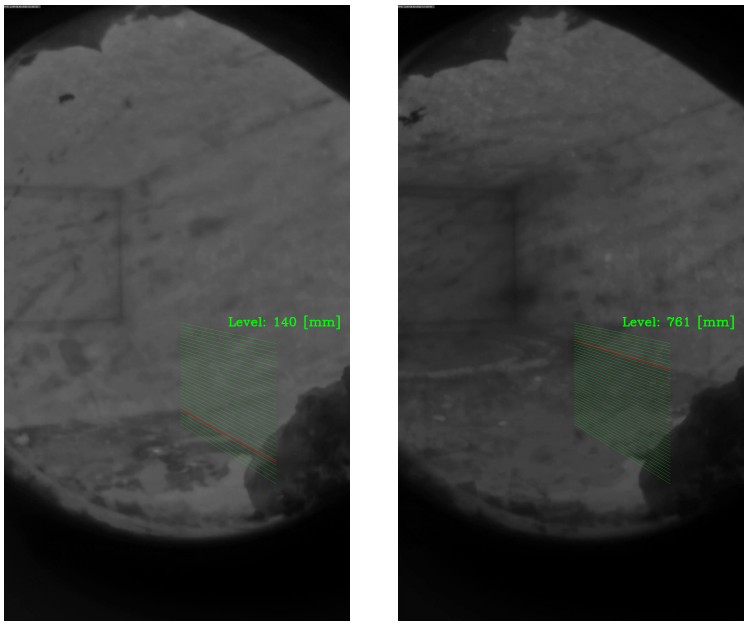

(a) (b)

Figure 29: Level measurement for the detected line in two different conditions

Testing of the Measurement System
As explained in 2.4.1 for the pre-processing step of the method two alternatives were evaluated: Gaussian filter and Bilateral filter. As declared in 2.4.2, two techniques were considered for the edge detection step: Canny operator and Otsu method. The combination of pre-processing and edge detection generates 4 approaches of the method. The tested approaches are listed in Table 1.

	Pre-Processing	+	**Edge Detection**
Approach 1	Gaussian Filter	+	Otsu Method
Approach 2	Bilateral Filter	+	Otsu Method
Approach 3	Gaussian Filter	+	Canny Detector
Approach 4	Bilateral Filter	+	Canny Detector

Table 1: The 4 tested approaches.

The tests were performed on videos ranging different illumination conditions. The tests evaluated measurement performances, robustness to light conditions and execution time. The type A measurement uncertainty for the 4 approaches was evaluated on a video in which the melt level is assumed to be constant. The illumination conditions don't change much throughout the whole video and can be considered the normal functioning conditions. The number of analysed frames is 454. A second video has been used to evaluate the method's dynamic performances for the 4 approaches in terms of robustness to illumination changes and tracking of the level variation. In the video the level is rising and different light conditions are present. The light conditions change approximately between 75 s and 105 s. Moreover the front door starts opening at 203 s. The door opening procedure implies the shutdown of the burners. The number of analysed frame is 444. The mean execution time for the analysis of a frame was computed as the mean of the execution times of the whole data-set (898 frames).

3. Results

The results of the experimental tests performed during the course of the research are presented in this section.

3.1. Contrast Enhancement Results

The results from the tests evaluating the two contrast enhancement techniques are shown. Two frames after grayscale conversion are illustrated in Figure 30 with their histograms. The outcome of the application of equalization technique is illustrated in Figure 31. The results of the histogram stretching technique are shown in Figure 32. The pixel intensities in histograms of Figure 30 are concentrated in a range that goes from 40 to approximately 90. The pixel intensities after equalization in Figure 31 are distributed across the whole scale [0, 255]. The pixel intensities after histogram stretching in Figure 32 are distributed on a range that goes from 0 to approximately 175.

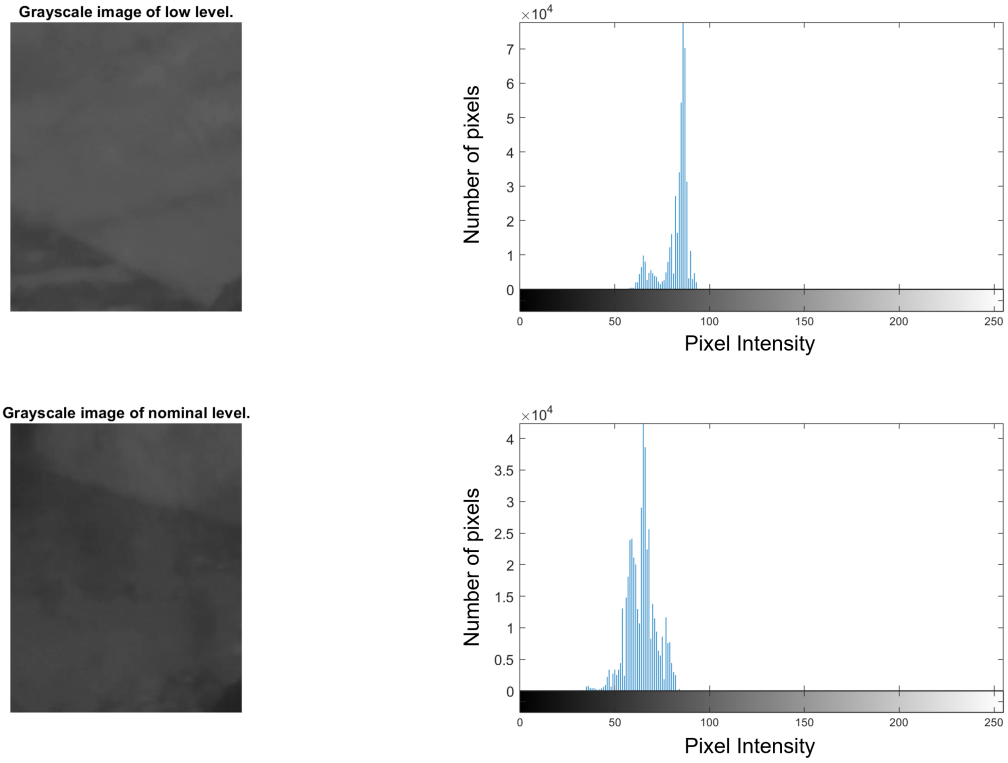

Figure 30: Cropped grayscale images and their respective histograms.

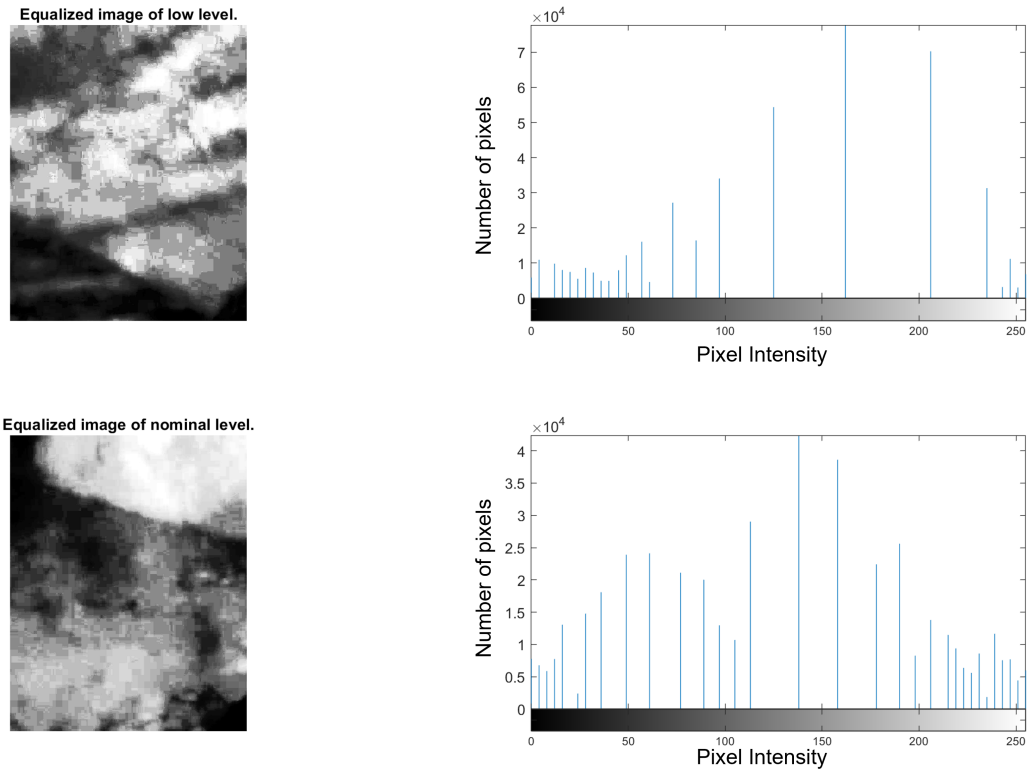

Figure 31: Cropped grayscale images and their respective histograms after Equalization.

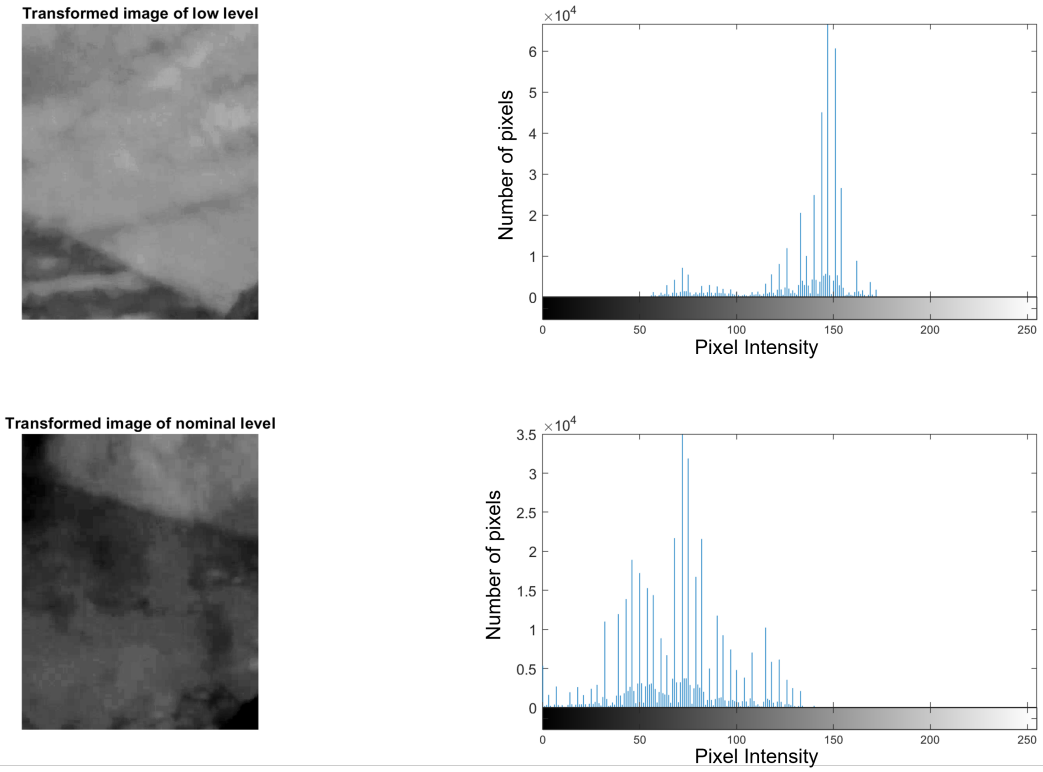

Figure 32: Cropped grayscale images and their respective histograms after histogram modification. Translation was performed with a value of 45. The gain used is 3,6.

3.2. Noise Reduction Results

The results from application of the different de-noising techniques are shown for a frame in Figure 33. The results are similar. With median filter in Figure 33b the noise is attenuated and the edge between melt and refractory wall is sharper. Noise with Gaussian filter 3x3 in Figure 33c is attenuated. The edge between melt and refractory wall after application of Gaussian 5x5 filter in Figure 33d is blurred. In the frame after application of Bilateral filter with values *sigmaSpace*=3 and *sigmaColor*=15 in Figure 33e the noise is attenuated and the edge is preserved.

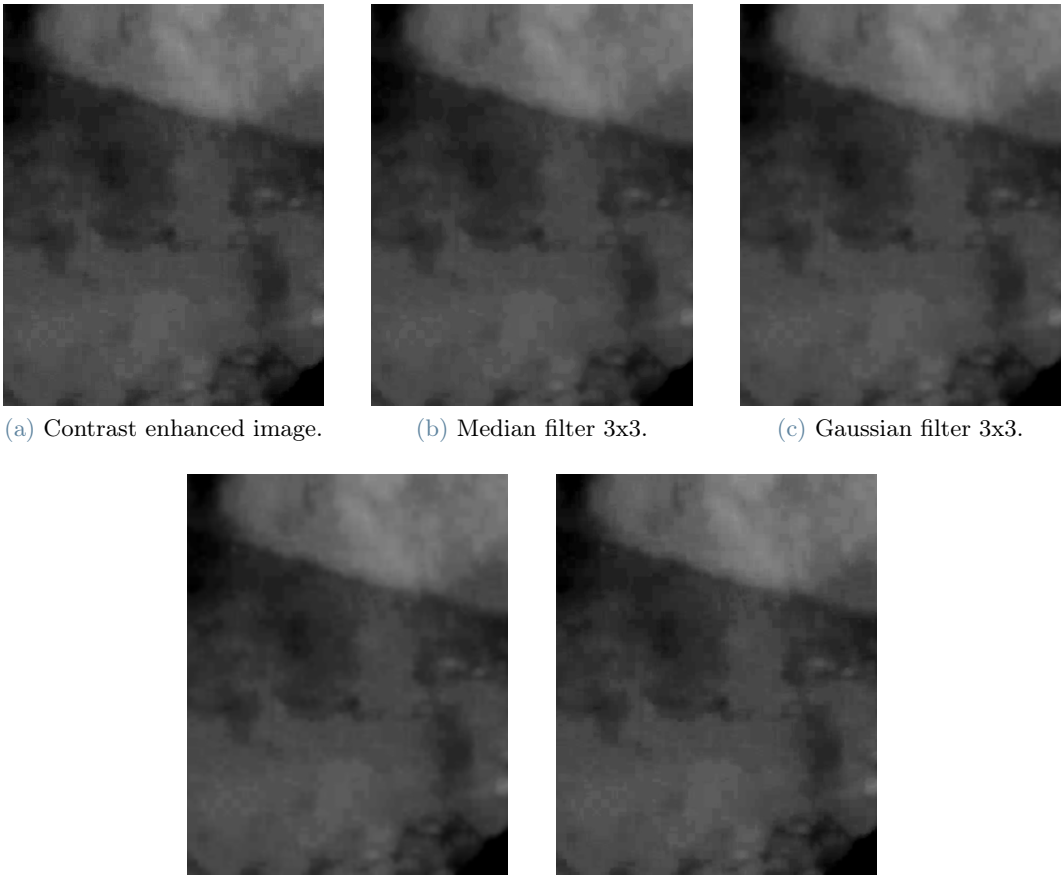

(a) Contrast enhanced image. (b) Median filter 3x3. (c) Gaussian filter 3x3.

(d) Gaussian filter 5x5. (e) Bilateral filter. *sigmaSpace=3*, *sigmaColor=15*.

Figure 33: Outcomes of de-noising for the 4 tested filters.

3.3. Edge Detection Results

Edges detected after applying Sobel 3x3, Sobel 5x5, Canny and Otsu methods are provided in Figure 34 for a frame. It is observed that the edges obtained with Sobel 3x3 in Figure 34b are imperceptible. Edges in Figure 34c from application of Sobel 5x5 are thick and undefined. Edges from Canny in Figure 34d are thin and discontinuous. On the other hand edges computed with Otsu method in Figure 34e are continuous and present some oscillations.

(a) Frame after pre-processing.

(b) Edges with Sobel gradient (3x3 kernel).

(c) Edges with Sobel gradient (5x5 kernel).

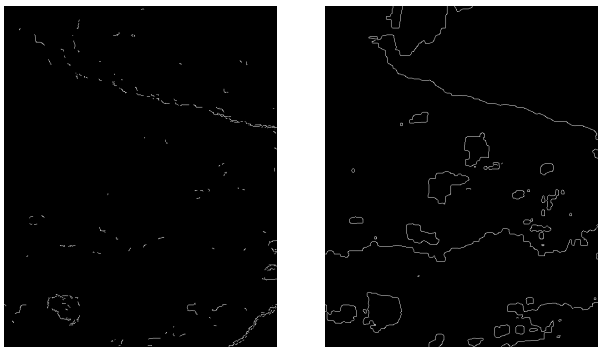

(d) Edges with Canny method.

(e) Edges with Otsu method.

Figure 34: Comparative result of Sobel, Canny and Otsu methods.

Figure 35 shows the operations sequence of the Otsu method for obtaining the edges in Figure 34e.

(a) Frame after pre-processing.

(b) Binary image after Otsu thresholding. *(Otsu threshold=61)*

(c) Edges extracted from binary image.

Figure 35: Application on a frame of Otsu thresholding for edge extraction.

3.4. Line Detection Results

Figure 36 compares the detected lines with Hough transform for a frame, when the edges are found with Canny operator or Otsu method.

(a) Edges extracted with Canny operator.

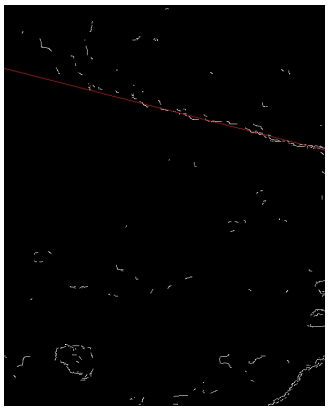

(b) Lines detected in (a) with Hough transform.

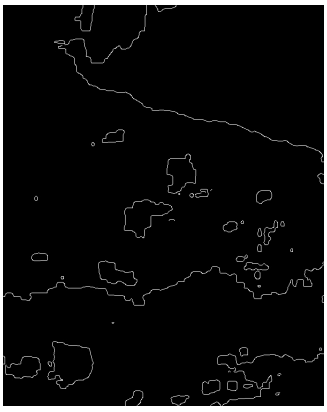

(c) Edges extracted with Otsu method.

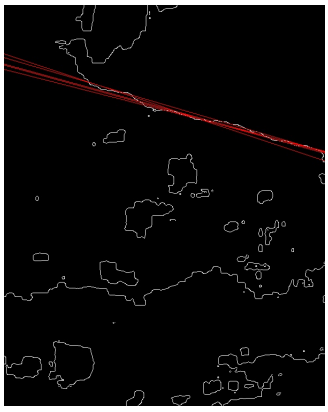

(d) Lines detected in (c) with Hough transform.

Figure 36: Lines detected with Hough transform (in red) for a frame in the two cases when the edges are extracted with Canny operator or Otsu method.

In Figure 36b a single line is detected upon applying Hough transform to Canny edges frame whereas multiple lines are detected for Otsu edges in Figure 36d.

3.5. Measurement Uncertainty Results

The results of the measurements for the 4 approaches are plotted in Figure 37. Table 2 contains mean value and measurement uncertainty for each approach. Four Gaussian distributions with the obtained mean values and standard deviations are plotted in red dashed line over the measurement distributions. The trends in Figures 37a and 37c for Otsu based approaches are not constant. On the other hand the trends in Figures 37e and 37g for Canny based approaches are constant.

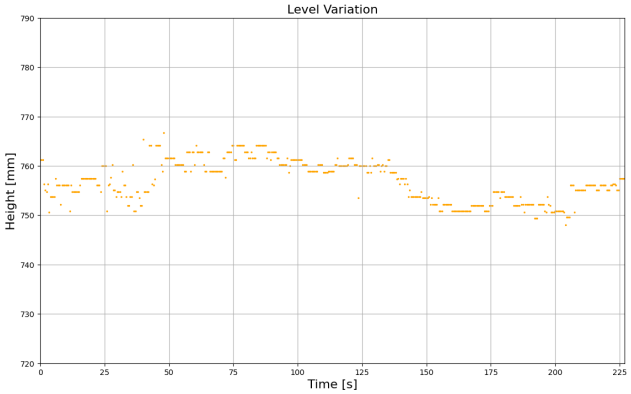

(a) Plot of level measured with approach 1.

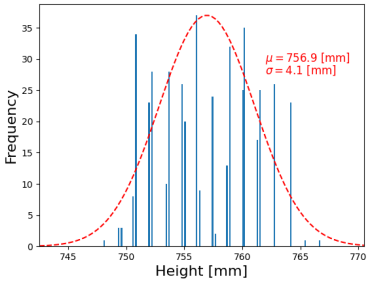

(b) Measurements distribution 1.

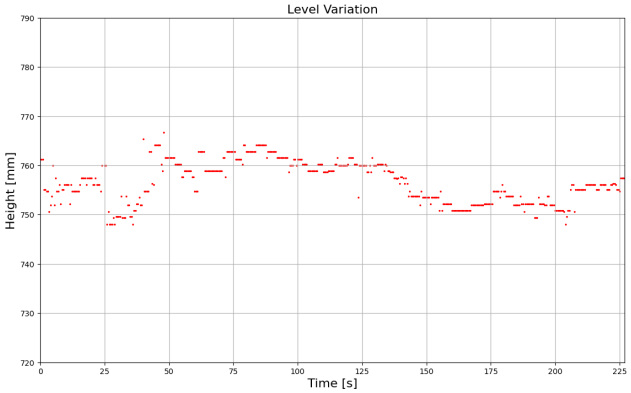

(c) Plot of level measured with approach 2.

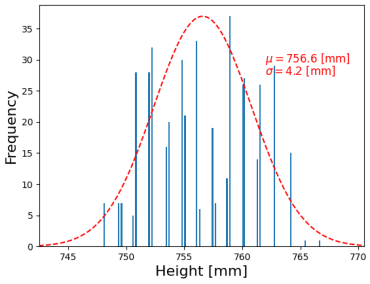

(d) Measurements distribution 2.

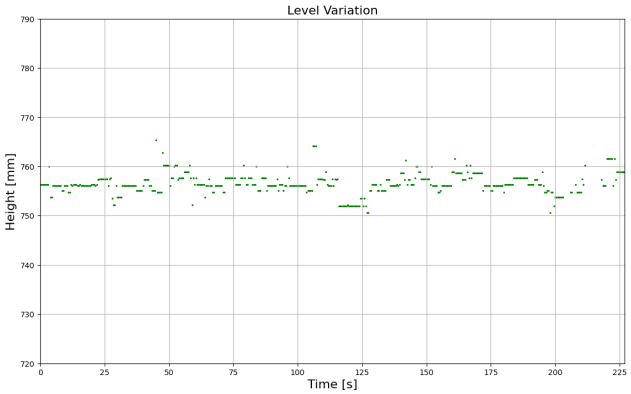

(e) Plot of level measured with approach 3.

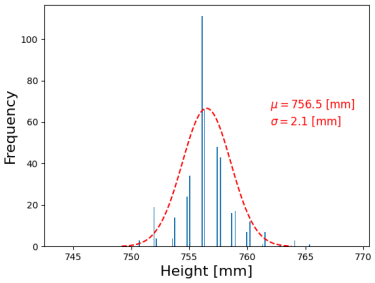

(f) Measurements distribution 3.

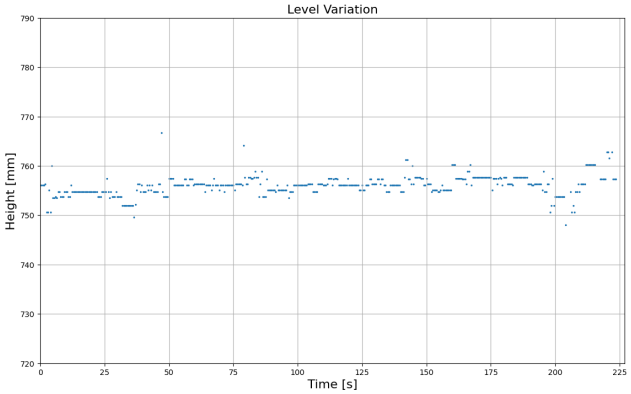

(g) Plot of level measured with approach 4.

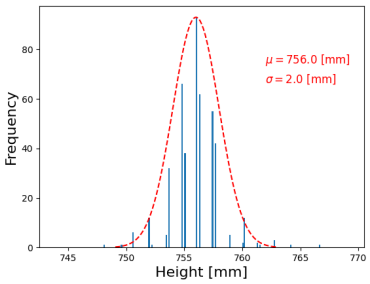

(h) Measurements distribution 4.

Figure 37: Plots of the level measured for the 4 approaches and relative measurements distributions.

	Mean Value	S.D. σ	u_A (k=3)
Approach 1	756.9 mm	4.1 mm	12.3 mm
Approach 2	756.6 mm	4.2 mm	12.6 mm
Approach 3	756.5 mm	2.1 mm	6.3 mm
Approach 4	756.0 mm	2.0 mm	6.0 mm

Table 2: Mean value, standard deviation and measurement uncertainty for the 4 approaches.

3.6. Dynamic Performances Results

The measurement results from the tests performed on the video with rising level and changes in the illumination conditions are shown in Figure 38. The window of time where the light conditions change in the video is highlighted by two vertical dashed lines in purple. The instant from which the front door starts opening is highlighted with the vertical dashed lines in light blue. For approaches 1 and 2 the first 5 s are evidenced by the green dashed lines. Overall the measured heights for the 4 approaches show a rising trend. In the purple window the measurement point are sparse as well as after the opening of the door.

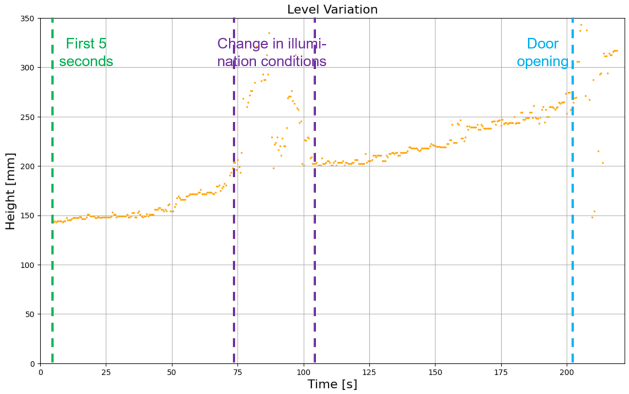

(a) Plot of level measured with approach 1.

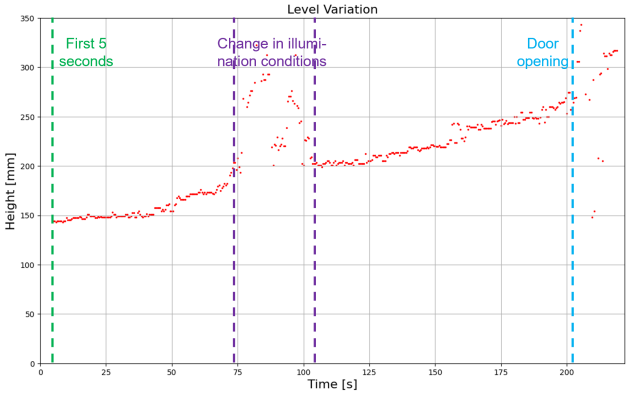

(b) Plot of level measured with approach 2.

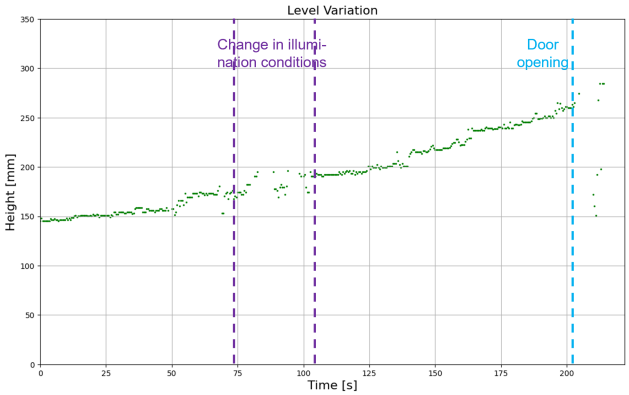

(c) Plot of level measured with approach 3.

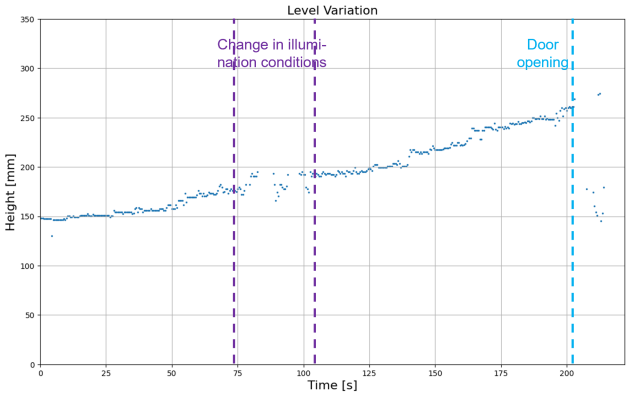

(d) Plot of level measured with approach 4.

Figure 38: Measurements of rising level for the 4 approaches.

3.7. Execution Time

The algorithm's mean execution time for a frame was computed for the 4 approaches. The computation was performed averaging the execution time of 898 frames. The results are collected in Table 3. Approach 2 with Bilateral filter and Otsu method requires the highest mean computation time for a frame. On the other hand approach 3 with Gaussian filter and Canny method requires the lowest mean computation time.

	Mean Execution Time
Approach 1	434 ms
Approach 2	772 ms
Approach 3	325 ms
Approach 4	369 ms

Table 3: Mean execution time for the 4 approaches.

4. Discussion

4.1. Contrast Enhancement

With reference to the results in 3.1 it was noticed that the significant intensity components in the histograms of the cropped grayscale frames were contained in a narrow range. The histograms in Figure 30 evidence that the intensity range goes approximately from 40 to 90. The whole scale from 0 to 255 isn't well exploited. The application of equalization technique on the frames of our data-set highly increased the contrast. The histograms in Figure 31 are stretched to the full [0,255] scale. However as can be observed in the two frames in Figure 31 the noise is magnified. Moreover the important features in the images aren't preserved. Regarding the second proposed histogram stretching method the histograms in Figure 32 evidence an acceptable enlargement of the intensity range. The range isn't as wide as the one obtained with equalization but noise results far less pronounced. Moreover the features appear to be preserved. For the considerations made the second method was chosen over equalization.

4.2. Noise Reduction

With reference to the images in Figure 33 the choice of the de-noising technique is discussed. The application of Median 3x3, Gaussian 3x3 and Gaussian 5X5 blurring shows almost negligible differences. Median filter was discarded because as stated in [20] it involves phenomena such as edge jitter which is to avoid in our case. Noise attenuation of the two Gaussian filters resulted similar (Figure 33c and 33d) but the one with kernel 5x5 has a higher blurring effect of the edges. Comparatively the Gaussian 3x3 is preferable. A slightly better result is given by the Bilateral filter (Figure 33e) which shows a better preservation of the level edge. This was best observed after the edge detection phase (Subsection 4.3). Gaussian 3x3 and Bilateral filters showed acceptable de-noising results and were chosen over the others.

4.3. Edge Detection

The results from the test for evaluation of edge detectors in 3.3 were compared. The edges found with Sobel detector with kernel size 3x3 resulted imperceptible as shown in Figure 34b. The result of enlarging the kernel size to 5x5 is presented in Figure 34c. The detector generates thick and spurious edges. This result is not usable for our case. On the other hand with Canny detector it was possible to obtain thin edges as shown in Figure 34d. The edges however aren't continuous. Still, this is an acceptable edge map considering that in the starting image (Figure 34a) there isn't a neat change of intensities in correspondence of the level. The result of the application of Otsu method for edge detection shown in Figure 34e is obtained by the sequence of operations in Figure 35. The edge map is composed of clearly visible and continuous edges. This method however is based on the assumption that the pixels belonging to the edge in the starting image (Figure 34a) have intensities similar to the Otsu threshold. This assumption needs verification. The performances of Canny method for edge detection are well known in literature [29]. Therefore Canny method was carried out in parallel

with Otsu method to verify its performances.

4.4. Line Detection

Figure 36 shows the result of the application of Hough algorithm to edge maps obtained with Canny and Otsu methods. It is observed that Hough algorithm returns more lines in the case of Otsu edge map (Figure 36d). In general edge maps obtained with Otsu method contain a large number of pixels and the edges are not perfectly straight lines. Due to this the vote counts are high and more lines get a number of counts larger than the threshold. The returned lines however are similar and in the neighbourhood of the edge. The detection of multiple lines was observed also when edges were obtained with Canny detector but in fewer cases.

4.5. Measurement Uncertainty

In the video used to estimate measurement uncertainty for the 4 approaches the level is assumed to be constant. Reference is made to the graphs in Figure 37. It is noticed that approaches 1 and 2 (Figure 37a and 37c), which use Otsu method for edge detection, follow a similar trend. It is observed that in both cases the measured heights don't follow a constant trend as would be expected. This shows that Otsu method is sensitive even to small variations in the light conditions. By comparison, the graphs of approaches 3 and 4 (Figure 37e and 37g) which use Canny detector appear more coherent with the analysed video. The measured heights in fact follow a trend which appears constant. This means that Canny detector is more robust to illumination changes. The effect of illumination changes can be observed in the measurements distribution of Figure 37b. It is pointed out that in fact the distribution relative to approach 1 doesn't follow the Gaussian characterized by computed mean and standard deviation. The same holds for the distribution relative to approach 2 in Figure 37d. On the other hand the distributions of the measurements from approaches 3 and 4 shown in Figure 37f and 37h are well described by Gaussian distributions. Furthermore in all 4 distributions it can be observed that there are gaps of approximately 1 mm between the columns. This effect has to be attributed to the discretization of the parameters space performed in the Hough algorithm. With regards to the effect of the pre-processing choice it is difficult to evaluate it in approach 1 and 2. For approaches 3 and 4 instead the effect is more evident. Approach 3 which uses Gaussian blur has a slightly higher standard deviation with respect to approach 4 which uses Bilateral filter. The results reported in Table 2 show that minimum value for uncertainty is obtained with approach 4 with the combination of Bilateral filter and Canny detector.

4.6. Dynamic Performances

With reference to the graphs of Figure 38 the dynamic performances of the 4 approaches are discussed. Results from approaches 1 and 2 in Figures 38a and 38b present the same behaviour. In the first 5 s they aren't able to provide any measurement. In the window of time that goes from approximately 75 s to 103 s the illumination in the furnace decreases significantly. The two approaches with Otsu based edge detection obtain clearly wrong measurements in this window, since the trend of the level is clear in the other time intervals. This is due to the fact that a decrease in illumination conditions implies the shifting of all intensities towards low values. Therefore the histograms used by Otsu technique result shrinked and are no longer bimodal. On the other hand the results from approaches 3 and 4 show less sensitivity to the change of illumination from 75 s to 103 s (Figures 38c and 38d). The measured heights in that window seem coherent with the trend of the measurements in the other intervals. It is also noticed from comparison between approach 3 and 4 that robustness to light conditions has very small correlation with the choice of the pre-processing filter (Gaussian or Bilateral). In the last part of the video at 203 s the front door opens and the process requires the shutdown of the burners. The light intensity levels become very low. As would be expected approaches 3 and 4 are no more able to detect borders. Approaches 1 and 2 instead still provide a few measures which are likely to be wrong due to the low intensity levels as for the interval from 75 s to 103 s. Overall approaches 3 and 4 have the best dynamic performances.

4.7. Execution Time

The results listed in Table 3 show that approaches 1 and 2 are slower than approaches 3 and 4. This is to be attributed to the edge maps obtained with Otsu method. Since the number of white pixels is higher with respect to edge maps obtained with Canny operator the Hough algorithm takes longer to process all the points. Mean execution times for approaches 3 and 4 are comparable. The slightly higher time of approach 4 with respect to 3 is due to the extra time required by the Bilateral filter.

5. Conclusions

A vision system for the measurement of aluminium level in casting furnaces has been developed. The system has been proven to be capable of detecting aluminium level in different operating conditions. Of the four approaches evaluated, 3 and 4 resulted to meet the expectations. Canny detector resulted to be robust to significative changes of lighting conditions while it was evidenced that the approaches 1 and 2 which are based on Otsu thresholding were too sensitive even to small variations. The set objective to obtain reliable measurements with uncertainty in the order of 5 mm was reached by approaches 3 and 4 which resulted to have uncertainty of respectively 6.3 mm and 6.0 mm with confidence level of 99.7%. The trade off is between accuracy and execution time which is respectively 325 ms and 369 ms. However both approaches have been considered suitable for on-line monitoring of the aluminium level height inside the casting furnace since the level change dynamics are slow. As expected the methods performed well when the illumination conditions were met. A future improvement could be the implementation of an algorithm for the adaptive adjustment of shutter speed based on illumination conditions. For further developments the use of different view angles for the camera could be investigated. A smaller view angle could focus only on the area of interest increasing the accuracy of the measurements.

References

[1] J.F. Grandfield and P.T. McGlade. Dc casting of aluminium: Process behaviour and technology. *Materials Forum*, pages Vol. 20: pages 27, 55, 1996.

[2] Atsumi Ohno. Continuous casting of single crystal ingots by the o.c.c. process. *JOM*, 38:14–16, 1986.

[3] J.M.A. Geldenhuis, D. Miller, B. Van Beek, J. Ndlovu, and K.T. Hara. Development of alternative techniques for matte level measurements in sulphide smelting furnaces. *International Platinum Conference 'Platinum Adding Value', The South African Institute of Mining and Metallurgy*, pages 25–26, 2004.

[4] Jin-Hong Lee, Jong-Yun Kim, Tae-Hong Park, and Sang-Eun Bae. Liquid level measurement by the detection of abrupt pressure changes in a tube in contact with a liquid surface. *J. Nucl. Fuel Cycle Waste Technol.*, Vol. 13:39–44, 2015.

[5] Weihua Zhang, Zesheng Ying, Shuo Yuan, and Zhengrong Tong. A fiber laser sensor for liquid level and temperature based on two taper structures and fiber bragg grating. *Opt. Commun.*, Vol. 342:243–246, 2015.

[6] Qing He, Hongji Meng, Zhenwei Hu, and Zhi Xie. Molten steel level detection from thermal image sequence based on the characteristics of adhesive flux. *IEEE TRANSACTIONS ON INSTRUMENTATION AND MEASUREMENT*, Vol. 68:3456–3467, 2019.

[7] Goohwa KIM, Hoyoung KIM, Kijang OH, Joonpyo PARK, Heetae JEONG, and Eui-Wan LEE. Level meter for the electromagnetic continuous casting of steel billet. *ISIJ International*, Vol. 43:224–229, 2003.

[8] Zhenwei HU, Ying CI, and Zhi XIE. Molten steel level measurement in tundish with heat transfer analysis. *ISIJ International*, Vol. 51:1674–1681, 2011.

[9] B. G. Thomas, M. A. Wells, and D. Li. Monitoring of meniscus thermal phenomena with thermocouples in continuous casting of steel. *TMS (The Minerals, Metals & Materials Society) Annual Meeting, San Diego, CA*, 2011.

[10] Aroba Saleem, Peter Ross Underhill, David Chataway, Terry Gerritsen, Afshin Sadri, and Thomas W. Krause. Electromagnetic measurement of molten metal level in pyrometallurgical furnaces. *IEEE TRANSACTIONS ON INSTRUMENTATION AND MEASUREMENT*, Vol. 69:3118–3125, 2020.

[11] Zhe Zhuang, Yu Zhang, Tonghao Zhou, and Shengchang Ji. Capacitance measurement of molten metal level in continuous casting system. *IEEE*, pages 419–423, 2020.

[12] Zhen Zhang, Yang Zhou, Haiyun Liu, Lili Zhang, and Huibin Wang. Visual measurement of water level under complex illumination conditions. *Sensors (Basel, Switzerland)*, 19, 2019.

[13] Gregor Bobovnik, Tim Mušič, and Jože Kutin. Liquid level detection in standard capacity measures with machine vision. *Sensors (Basel, Switzerland)*, 21, 2021.

[14] Fars Esmat Samann. Real-time liquid level and color detection system using image processing. *Academic Journal of Nawroz University*, 2018.

[15] Yan-Ting Lin, Yi-Chun Lin, and Jen-Yu Han. Automatic water-level detection using single-camera images with varied poses. *Measurement*, 127:167–174, 2018.

[16] Ti-Ho Wang, Ming-Chih Lu, Chen-Chien Hsu, Cheng-Chuan Chen, and Jia-Dong Tan. Liquid-level measurement using a single digital camera. *Measurement*, 42:604–610, 2009.

[17] S. Chakravarthy, R. Sharma, and R. Kasturi. Noncontact level sensing technique using computer vision. *IEEE Transactions on Instrumentation and Measurement*, 51(2):353–361, 2002.

[18] Rafael C. Gonzalez and Richard E. Woods. *Digital Image Processing (3rd Edition)*. Prentice-Hall, Inc., USA, 2006.

[19] A. Novini. Fundamentals of machine vision lighting. In *Proceedings of WESCON '93*, pages 38–46, 1993.

[20] James Coady, Andrew O'Riordan, Gerard Dooly, Thomas Newe, and Daniel Toal. An overview of popular digital image processing filtering operations. In *2019 13th International Conference on Sensing Technology (ICST)*, pages 1–5, 2019.

[21] Richard O. Duda and Peter E. Hart. Use of the hough transformation to detect lines and curves in pictures. *Commun. ACM*, 15:11–15, 1972.

[22] Aritz Legarda, Alberto Izaguirre, Nestor Arana, and Aitzol Iturrospe. Comparison and error analysis of the standard pin-hole and scheimpflug camera calibration models. In *2013 IEEE 11th International Workshop of Electronics, Control, Measurement, Signals and their application to Mechatronics*, pages 1–6, 2013.

[23] Z. Zhang. A flexible new technique for camera calibration. *IEEE Transactions on Pattern Analysis and Machine Intelligence*, 22(11):1330–1334, 2000.

[24] G. Bradski. The OpenCV Library. *Dr. Dobb's Journal of Software Tools*, 2000.

[25] Christopher Kanan and G. Cottrell. Color-to-grayscale: Does the method matter in image recognition? *PLoS ONE*, 7, 2012.

[26] Hojat Yeganeh, Ali Ziaei, and Amirhossein Rezaie. A novel approach for contrast enhancement based on histogram equalization. In *2008 International Conference on Computer and Communication Engineering*, pages 256–260, 2008.

[27] Sylvain Paris, Pierre Kornprobst, Jack Tumblin, and Frédo Durand. A gentle introduction to bilateral filtering and its applications. In *SIGGRAPH '08*, 2008.

[28] Syed Jahanzeb Hussain Pirzada and Ayesha Siddiqui. Analysis of edge detection algorithms for feature extraction in satellite images. In *2013 IEEE International Conference on Space Science and Communication (IconSpace)*, pages 238–242, 2013.

[29] Mamta Juneja and P. Sandhu. Performance evaluation of edge detection techniques for images in spatial domain. *International Journal of Computer Theory and Engineering*, pages 614–621, 2009.

[30] Nobuyuki Otsu. A threshold selection method from gray level histograms. *IEEE Transactions on Systems, Man, and Cybernetics*, 9:62–66, 1979.

[31] Sunil L. Bangare. Reviewing otsu's method for image thresholding. 2015.

[32] Ningbo Zhu, Gang Wang, Gaobo Yang, and Weiming Dai. A fast 2d otsu thresholding algorithm based on improved histogram. In *2009 Chinese Conference on Pattern Recognition*, pages 1–5, 2009.

[33] Zezhong Xu, Bok-Suk Shin, and Reinhard Klette. Accurate and robust line segment extraction using minimum entropy with hough transform. *IEEE Transactions on Image Processing*, 24(3):813–822, 2015.

[34] Yu Zheng and Bingxin Xia. High precision fast line detection of alignment and coupling for planar optical waveguide device. *Optik*, 145:519–528, 2017.

[35] N. Aggarwal and W.C. Karl. Line detection in images through regularized hough transform. *IEEE Transactions on Image Processing*, 15(3):582–591, 2006.

[36] Ming Zhang. On the discretization of parameter domain in hough transformation. In *Proceedings of 13th International Conference on Pattern Recognition*, volume 2, pages 527–531 vol.2, 1996.

[37] Pio G. Iovenitti, William Thompson, and Manmohan Singh. Three-dimensional measurement using a single image. *Storage and Retrieval for Image and Video Databases*, 1996.

Abstract in lingua italiana

La misurazione accurata del livello di alluminio fuso nei processi di colata continua è una questione importante che influisce sulla qualità del prodotto finale e sull'efficienza del processo. Il lavoro presentato è diretto allo sviluppo di un sistema di visione a telecamera per la misurazione del livello dell'alluminio all'interno di una fornace. La superficie dell'alluminio fuso e le pareti refrattarie interne del forno hanno valori di intensità luminosa diversi. All'interfaccia formano un bordo che può essere utilizzato per identificare una linea utilizzando le tecniche di visione artificiale esistenti. È stato sviluppato un algoritmo per determinare il livello di alluminio fuso dalla linea rilevata. Il sistema di riferimento per la misurazione del livello si basa sulla dimensione e la posizione relativa delle caratteristiche note del forno nel campo visivo della telecamera. L'algoritmo è in grado di fornire misure in tempo reale del livello di alluminio per diverse condizioni di illuminazione. Gli esperimenti sul campo hanno dimostrato che il metodo è in grado di ottenere misure del livello con un errore di misurazione di 6 mm con un livello di confidenza del 99,7%.

Parole chiave: misurazione del livello, livello di alluminio fuso, sistema video, visione artificiale

Acknowledgements

I wish to thank professor Tarabini for the opportunity to conduct this thesis. A big thanks goes to Fabio and Yuvan for always supporting me in the development of this work.